Hydroelastic Impacts of Deformable Wedges

Riccardo Panciroli

Abstract This work investigates the slamming phenomenon experienced during the water entry of deformable bodies. Wedges are chosen as reference geometry due to their similarity to a generic hull section. Hull slamming occurs when a ship re-enters the water after having been partially or completely lifted out the water. There are three more cases commonly defined as slamming phenomena: bow-flare, wet-deck and green water slamming. These are all special cases of the general topic of water entry of a body. While the analysis of rigid structures entering the water has been extensively studied in the past and there are analytical solutions capable of correctly predicting the hydrodynamic pressure distribution and the overall impact dynamics, the effect of the structural deformation on the overall impact force is still a challenging problem to be solved. In fact, in case of water impact of deformable bodies, the dynamic deflection could interact with the fluid flow, affecting the hydrodynamic load. This work investigates the hull-slamming problem by experiments and numerical simulations of the water entry of elastic wedges impacting on an initially calm surface with pure vertical velocity. The objective is to determine an accurate model to predict the overall dynamics of the wedge and its deformations. More than 1,200 experiments were conducted by varying wedge structural stiffness, deadrise angle, impact velocity and mass. On interest are the overall impact dynamics and the local structural deformation of the panels composing the wedge. Alongside with the experimental analysis, numerical simulations based on a coupled Smoothed Particle Hydrodynamics (SPH) and FEM method are developed. Ranges of applicability of a simplified model neglecting the air are found. The results provide evidence of the mutual interaction between hydrodynamic load and structural deformation. It is found a simple criterion for

R. Panciroli (✉)
Alma Mater Studiorum, Università di Bologna, Viale del Risorgimento 2, 40136, Bologna, Italy
e-mail: riccardo.panciroli@unibo.it

S. Abrate et al. (eds.), *Dynamic Failure of Composite and Sandwich Structures*,
Solid Mechanics and Its Applications 192, DOI 10.1007/978-94-007-5329-7_1,

the onset of fluid structure interaction (FSI), giving reliable information on the cases where FSI should been taken into account. The occurrence of ventilation and cavitation varying the impact parameters are also outlined.

1 Introduction

When a vessel sails in rough seas, its forefoot can rise above the water surface. As the vessel re-enters the water, impulsive pressures are imparted to the hull structure due to the relative motion of the sea and ship. In these cases the hull literally slams into the water surface. The duration of the slamming event is in the order of milliseconds. These loads might damage the entire ship or, because of their short duration, excite dynamic response of the local structure of the hull and cause vibrations. This work focuses on hull slamming; however, there are three more phenomena that are defined as slamming in marine applications: (1) the impact of the bow on water induced by the ship motions in waves, (2) the horizontal impact of steep waves or breaking waves on the ship hull and (3) the water impact induced by water run-up and green water on the deck.

1.1 Theoretical Studies

It is of major interest for engineers to find an analytical solution capable of providing the hydrodynamic load and the impact pressure during a slamming event, since it can be easily used during the design process. This section describes the analytical methods developed to study the water entry of rigid bodies.

The first analytical solution to solve the impact dynamics of rigid bodies entering the water was presented by Von Karman [1], who developed a formula capable to predict the maximum force acting on a rigid body entering the water, in order to make a stress analysis on the members connecting the fuselage with the floats of a seaplane. As example, to study the water entry of a rigid wedge, Von Karman considered a wedge of unit thickness, mass M, and deadrise angle β entering the water with initial velocity V_0. Von Karman's work is based on some simplification, i.e.: (1) inviscid and irrotational flow, (2) surface tension, gravity and structural elasticity effect neglected, (3) no air entrapped. In this method, as the body hits the water it is assumed that the mass of a half disk of water of radius r is moving with the wedge (as shown in Fig. 1), resulting in an added mass $m = \frac{\pi}{2}\rho r^2 = \frac{\pi}{2}\rho\frac{\xi^2}{tan^2(\beta)}\gamma^2$, where γ is a coefficient accounting for the water pile up at the intersection with the free surface that varies with the deadrise angle. The value of γ can be evaluated as suggested in [2], for example. In this model, velocity and acceleration of the body are given by:

$$\dot{\xi} = \frac{V_0}{1 + \frac{\pi}{2}\rho\frac{\gamma^2\xi^2}{Mtan^2(\beta)}} \quad ; \qquad \ddot{\xi} = \frac{\pi\rho\gamma^2}{MV_0tan^2(\beta)}\xi\dot{\xi}^3 \tag{1}$$

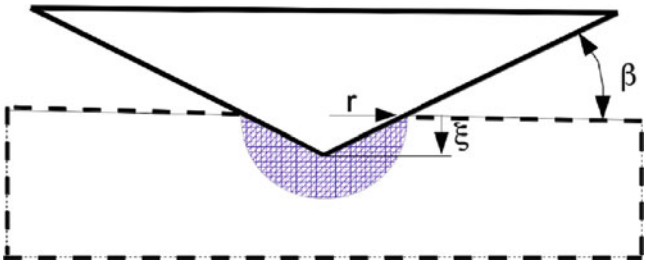

Fig. 1 Von Karman's momentum approach. Where β is the deadrise angle, ξ the penetration depth, r the wet distance from the wedge edge. The cross-hatched region represents a half disk of water of radius r moving with the wedge

In von Karman's model (Eq. 1), the impact force reaches its maximum value

$$F^* = \left(\frac{5}{6}\right)^3 \frac{V_0^2}{tan(\beta)} \sqrt{\frac{2\pi}{5}\rho M \gamma^2} \tag{2}$$

when the velocity is

$$\dot{\xi}^* = \frac{5}{6} V_0 \tag{3}$$

the penetration depth is

$$\xi^* = \sqrt{\frac{2M}{5\pi\rho\gamma^2}} tan(\beta) \tag{4}$$

and the time is

$$t^* = \frac{16}{15} \frac{\xi^*}{V_0} \tag{5}$$

Equation 2 shows that the maximum force increases with the square of the velocity and the square root of the mass of the wedge. F^* is inversely proportional to $tan(\beta)$ so that it decreases as β increases and it becomes infinite as the deadrise angle tends to zero. When β becomes small, r becomes very large, the added mass becomes infinite and the wedge stops instantly. Equation 3 shows that the velocity is 5/6 times the initial velocity when the force reaches its maximum. Equation 4 shows that the penetration depth at that particular instant is proportional to the square root of the mass and to $tan(\beta)$ ($tan(\beta) = 0$ implies no penetration). Combining Eqs. 4 and 5 gives

$$t^* = \frac{16}{15} \frac{\tan(\beta)}{V_0} \sqrt{\frac{2M}{5\pi\rho\gamma^2}} \tag{6}$$

This shows that the force reaches its maximum at a time that is inversely proportional to the initial velocity and increases with $tan(\beta)$. Figure 2 shows the overall acceleration and velocity of a wedge of 20 Kg per unit with entering the water at 4 m/s for various deadrise angles. It is shown that decreasing the deadrise angle from 30° to 5° leads to an increase of the maximum acceleration and a reduction of the characteristic time t^*.

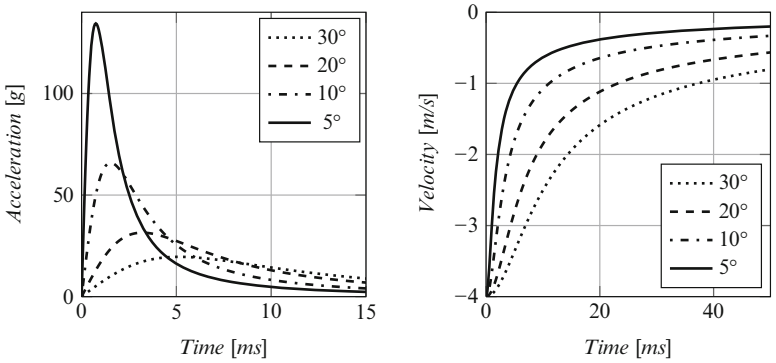

Fig. 2 Von Karman solution. Acceleration and Velocity of a wedge varying the deadrise angle β. Total wedge mass: 20 kg per unit width

Wagner [3] later extended Von Karman's method to predict the pressure distribution at the fluid/structure interface during the impact. In this model, the pressure along the wedge is given by:

$$\frac{p(x)}{\rho} = \ddot{\xi}\sqrt{r^2 - x^2} + \frac{\pi}{2}\frac{\dot{\xi}^2 r}{tan(\beta)\sqrt{r^2 - x^2}} - \frac{1}{2}\frac{\dot{\xi}^2 x^2}{r^2 - x^2} \tag{7}$$

Equation 7 shows that the pressure becomes infinite when β tends to zero and there is a singularity near the end when x tends to r. The maximum impact pressure p_{max} is obtained by defining $dp/dc = 0$ and assuming the acceleration of the body $\ddot{\xi}$ to be negligible. This gives

$$p_{max} = \frac{1}{2}\rho V^2 \left[1 + \frac{\pi^2}{4} cot^2\beta\right] \tag{8}$$

which occurs at the location

$$x = L\left[1 - \frac{4\tan^2\beta}{\pi^2}\right]^{\frac{1}{2}} \tag{9}$$

since p_{max} occurs some time t after the instant of impact t_0, V is used in Eq. 8 since it might not be the impact velocity V_0. At the keel of the wedge, $x = 0$. From Eq. 7, the impact pressure at that point is

$$p_{keel} = \frac{1}{2}\,\rho\, V^2\,\pi\, cot(\beta) + \ddot{\xi}\,\rho\, L \tag{10}$$

if $\ddot{\xi}$ can be neglected,

$$p_{keel} = \frac{1}{2}\,\rho\, V^2\,\pi\, cot(\beta) \tag{11}$$

These analytical models were developed for the analysis of the water entry of rigid bodies and are not capable of accounting for hydroelastic effects, since the changes of the fluid motion due to the structural deformation are not accounted. Thus, in the present work, Wagner and Von Karman solutions will be used to validate the numerical model in the case of slamming of rigid bodies, while the validated numerical model will be used to study the water entry of deformable wedges, since hydroelastic effects might appear.

Since Wagner developed the first analytical solution to evaluate the pressure during water-entry problems, much effort has been devoted to slamming problems, resulting in an impressive amount of papers: more than 200 papers were listed in the Ship Structure Committee report SSC-385 [4].

In the literature, many analytical methods extend Wagner's method to different shapes (e.g. [2, 5]) and are very effective when dealing with the water entry of simple-shaped structures impacting the surface with pure vertical velocity. However, these analytical models are limited to the analysis of simple-shaped bodies impacting onto a free and initially calm surface. Yettou [6] developed an analytical solution to symmetrical water impact problems, showing a very good agreement between experimental results and analytical solutions of the water entry of rigid wedges. Some of these solutions are even capable of accounting for oblique impacts (e.g. [7–9]). It is reported that there are particular conditions (entry velocity, deadrise angle and tilt angle) where the fluid detaches from the wedge apex (i.e. the keel) introducing difficulties in evaluating the pressure at the interface by analytical formulations. Chekin [10] concluded that there was only one unique combination of wedge angle and impact angle from which no separation of flow from the vertex would occur. For a given wedge and wedge orientation, any other impact angle would force separation. Defining U_0 the horizontal velocity and W_0 the vertical velocity, the ratio $\frac{U_0}{W_0}$ at which the flow separation appears is less for bodies of larger deadrise angles. For small asymmetric impacts, the cavity flow that generates at the apex during the water entry is very small. Furthermore, the flow that separates from the apex quickly re-attaches to the wedge. A symmetric body impacting with horizontal velocity will produce a flow similar to asymmetric impact with only vertical velocity when rotation about the x-axis is not allowed. In [7], Judge at al. performed experiments on wedges where asymmetry and horizontal impact velocity are present and compared the results with an analytical solution, showing good agreement for low angles of asymmetry and small ratios of horizontal to vertical impact velocity.

Some models are even capable of accounting for the coupling between the fluid motion and the structural deformation [11–15]. However, in order to fully describe impact forces and resulting structural response, other different phenomena (like trapped air, hydroelastic interaction, compressibility effects, and non-linear free surface mechanics) must be considered. These phenomena need further investigation. Accurate prediction methods for hydrodynamic loads are needed in order to reduce the probability of structural failure.

1.2 Hydroelastic Effects in Water Impact Problems

The analytical models developed for rigid bodies might not be used to study the water entry of deformable bodies since the structural deformation might change the hydrodynamic pressure and the impact dynamics due to hydroelastic effects. This section gives a brief review about the known methods to study hydroelasticity during slamming. Experimental, analytical and numerical approaches are presented.

Hydroelasticity is the dynamic interaction between water and a structure (sometimes called fluid-structure interaction). Water entry is only one example of it. Faltinsen in his review [16] on hydroelastic slamming show that it is common to use an equivalent pressure resulting in the same maximum strain in the structure reached during the dynamic event, but has no physical meaning and the resulting pressure load would be an order of magnitude smaller than the maximum physical pressure.

Due to the mutual interaction between the fluid motion and the structural deformation, the hydrodynamic loads that elastic bodies are subjected during the water entry might differ from the loads acting on rigid bodies [17]. The concept is that the impact pressure is related to the movement of the impact region with respect to the water [18]. In particular, as mentioned in [14], the evolution of the wetted body area in time is an important characteristic of the impact, which strongly affects the magnitude of the loads. Elastic structures with low deadrise angles are the most subjected to changes in the impact dynamics respect to rigid structures, since a small deflection of the structure might result in a big difference of the wetted surface and consequently the hydrodynamic load. Such problems are still difficult to analyze and compute.

Carcaterra and Ciappi [19] studied the water entry problem of elastic wedges simplifying the deformable wedge as two rigid plates connected by a rotational spring of constant stiffness. They show how the hydrodynamic force is affected by the deformation of the wedge. It was found that during the initial phase of the impact the deadrise angle decreases due to the structural deformation. When the deadrise angle becomes smaller, the wetted surface is increased and an increment of the hydrodynamic load, with respect to the rigid wedge case, is observed. When the wetted front crosses the center of gravity line, an opposite moment contribution arises that tends to contrast the deadrise decrement. Alternate closing and opening of the wedge was predicted. They showed that this phenomenon could be observed only if the natural period of oscillations is small compared to the characteristic time of application of the hydrodynamic force. They observed that the mass of the plates composing the wedges has an influence on the stresses at the beginning of the impact, when the inertia induces the deadrise angle to decrease, even if the hydrodynamic load itself is pushing the wedge to close and increase its deadrise angle. A similar effect was experimentally found by Arai and Miyanki [20].

Kapsenberg [21] reported that, in case of hydroelastic phenomena, the magnitude of the deformation of an elastic body might be lower than the one expected from classical beam theory and neglecting hydroelastic effects can, in an extreme case, result in an over-prediction of the deformation (hence the stress) by a factor of 10.

Several scientists [16, 20–29] investigated the water impact of elastic structures, showing that the the relative importance of the elasticity of the beam on the hydrodynamic force is governed by deadrise angle, panels thickness and impact velocity. Hydroelastic effects are relevant when the relative angle between the body and the surface of the fluid is small, and if the duration of the impact is short relative to the resonance period of the structure. Hirdaris and Temarel [30] suggest that particle-based methods, as other numerical methods, are expected to become increasingly used in the future, but currently suffer of lack of computational efficiency. Further studies and validations on its applicability to water entry problems are needed.

Many solutions of water-entry problems are available and many are very effective in dealing with the water entry of complex geometries, sometimes even considering oblique impacts (e.g. [7]), but most deal with rigid structures. To study more realistic situations, many numerical methods capable of coupling the fluid dynamics with the structural response have been used [11, 12, 15, 25, 31].

Seddon and Moatmedi [32] review the literature on the water entry problems for aerospace structures from 1929 to 2003 and show that very few efforts were made to develop solutions for non-vertical impacts, three-dimensional bodies, or deformable bodies. The majority of the work on these problems is experimental. They suggest that Smoothed Particle Hydrodynamics (SPH) can possibly be a tool to study these problems, but that a large amount of work is required to validate such models. One of SPH's major advantages is the ease of treating fluids presenting a free surface, together with the possibility to interact with FEM models, while its major limitation is the very expensive computational time due to the high number of particles needed to model the fluid, which limits its application to relatively small two dimensional models [33–36]. For example, in [35] 21 millions particles are needed to obtain results similar to Wagner's solution for the water entry of a rigid wedge. Anghileri et al. [37] used the SPH method to study the water entry of a rigid cylinder and a rigid wedge, showing a good prediction of the impact force.

Shao [38] performed a sensitivity analysis by refining the particle spacing. It was found that the spatial resolution can have a relatively large influence on the flow in the water splash-up region (the water entry produces a water jet piling up the wedge panels during impact, see e.g. [39]), but it has less influence on the falling velocity of the object and the fluid forces. The finer the particle resolution is, the better the detailed flow structures can be resolved, but at the cost of more computational time. For the pressure evaluation at the fluid/structure interface, many articles show results that are inaccurate and lack details, to the point that this technique cannot be considered to be fully suitable for this purpose [34–36]. In general, the pressure values suffer noise due to numerical fluctuations. An averaging therapy on the pressure field has been recently proposed in the literature (see i.e. [40]). Molteni and Colagrossi [41] proposed the introduction of a proper diffusive term in the continuity equation to increase the smoothness and the accuracy of pressure profile. They showed that this corrective method does not alter the match of the numerical solution with the analytical one. However, no fluid/structure interaction problems are treated in their study. Kapsenberg [21] reported that SPH

is numerically a very robust method and impressive results are obtained for very violent phenomena. However, work on verification of the results (convergence with respect to particle size and time step) is not yet at the level of the normal CFD. Kapsenberg also reports that the main problems related to the SPH method are difficulties in correctly reproducing the pressures wave propagation and a robust treatment of the fluid/structure interface, while computer requirements are an order of magnitude higher than for classic CFD methods.

During the water entry of flat-bottom structures with high velocity, air can be trapped in between the fluid and the structure. The next section describes this phenomenon.

1.3 Air Cushioning Effect in Water Entry

Trapping of air in the fluid during the water impacts is common in case of impact of flat-bottom structures [43]. This section describes its relieving effects on the maximum impact pressure.

In [44] two-dimensional impact tests of a rigid flat-bottom model indicates that the maximum impact pressure is nowhere near the theoretical infinitely large hydrodynamic pressure or near the theoretical acoustic pressure. With the assumption that no air is trapped in the fluid during the slamming event of a flat structure, an approximate value of the maximum impact pressure is [45]:

$$p_{max} = \rho c V_0 \tag{12}$$

where p is the pressure, ρ is the fluid density, c is the speed of sound in the fluid, and V_0 is the impact velocity. However, evidences resulting from investigations reveal that the impact of flat structures is cushioned by the presence of trapped air between the falling body and the water. If all the air is forced to escape during a flat-bottom drop, the air velocity must be infinite just before impact occurs. Consequently some air is trapped between the water and the structure: as the body approaches the surface of the water and the air cannot escape fast enough, the pressure deforms the surface of the water before contact is made. Then, a large air bubble is trapped under the body. This causes the impact pressure to be reduced. Air trapping is maximum for a flat-bottom structure, but it appears (with lower magnitude) for deadrise angles up to about 10°. The cushioning effect of the compressible air trapped between the impact body and the water surface reduces the impact pressure to about one-tenth of the acoustic pressure predicted by Eq. 12. Evidence from Chuang's investigation [18] supports the thesis that Wagner's hydrodynamic impact theory does not apply to the impact of wedge-shaped bodies with small deadrise angles. Furthermore, Chuang experiments showed that a deformable body affords considerable relief from the impact load.

1.4 Experimental Studies

This section introduces some of the experimental studies on the water entry found in the literature. Most of them investigate the water entry of stiff bodies. The major attention is given to the evaluation of the impact dynamics and the pressure at the fluid/structure interface (e.g. [37]). For example, Engle [46] studied the water entry of rigid wedges measuring the pressure at the fluid/structure interface. Results based on peak pressures at different impact velocities compared well with Wagner's theory. Some authors attempted to experimentally investigate the parameters affecting hydroelasticity during slamming. Several scientists [24–27] reported that the water entry of deformable bodies is affected by various parameters: stiffness of the structure, presence of entrapped air between the structure and the water surface. It reported that the ratio between the impact duration and the period of the first dry mode of vibration is the key factor in deciding when the analysis of the structural response should include elastic deformations.

Faltinsen [16,22] showed that, due to hydroelasticity, cavitation may occur since pressures becomes negative relative to atmospheric pressure during the second half of the first wet natural oscillation period; ventilation might also appear, i.e. air can be caught in an air pocket in the water leading the air flow to interact with the water flow. Recently Huera-Huarte [47] experimentally studied the hydrodynamic load on panels entering the water at speeds higher than 5 m/s and low deadrise angles, showing that for angles lower than 5° air entrapment is important and the analytical solutions tend to overestimate the hydrodynamic loads.

Results found in the literature show that there are particular conditions where hydroelastic, air entrapment, cavitation and ventilation phenomena might occur during slamming. However, a reliable tool to predict the occurrence and the magnitude of such phenomena is missing.

1.5 Scope of Present Investigation

As shown in the previous literature review, there are many complicating factors related to hydroelastic effects. Many authors concentrated on the experimental evaluation of the pressure variation due to the structural deformation during the water entry. The primary objectives of this work are:

- Experimentally evaluate the hydroelastic effects by experiments where the dynamic interaction between the structural deformation and the fluid motion is high.
- Develop a numerical model to study the water entry of deformable bodies which can correctly predict the overall impact dynamics and the impact-induced stresses and validate it by comparison with the experimental results.

This study presents an extended experimental campaign on the water entry of deformable wedges. Experiments investigate the water-entry of composite and aluminum flexible wedges varying thickness, deadrise angle and impact velocity. The objective is to develop a reliable formula capable of estimating the maximum stress reached during the water entry of deformable bodies.

Results of the impact-induced accelerations are compared with analytical solutions for rigid structures: assuming that the wedge is rigid, the impact dynamic can be evaluated by Von Karman's approach, while the pressure distribution along the edge can be determined using Wagner's formula. This pressure can be used to calculate the stresses in the panels provided that deflections remain small and do not induce changes in the fluid flow. This study examines cases where the deformation of the wedge is very large. This affects the fluid flow and consequently the pressure distribution along the edge, introducing hydroelastic effects. The impact-induced acceleration is recorded by an accelerometer while strain gauges located at various locations on the wedge measure the overall local deformations. Alongside with the experimental campaign, numerical simulations are developed by a coupled SPH/FEM numerical model and the computed structural deformations are compared with the experimental results.

This research initially validates the coupled FEM/SPH model by analyzing its capability to correctly reproduce the pressure waves propagation and the overall fluid motion. Later, it investigates the water-entry problems of rigid bodies, whose results are compared with Von Karman and Wagner's analytical solutions, showing that SPH is actually capable of correctly simulating the impact dynamics. The accuracy of the solution in terms of pressure at the fluid-structure interface was found to be highly influenced by various parameters like: element size, artificial bulk viscosity and non-reflecting boundary conditions. Once the solution method has been validated, the research moves to the investigation of hydroelastic effects on the impact dynamics and structural deformation. Numerical results are compared with experiments about water-entry of elastic wedges of varying thickness, deadrise angle and impact velocity.

Experimental results show that the relative importance of hydroelasticity is strictly related to the ratio between the time necessary for the structure to get completely wet during the water entry (also called wetting time) and the natural period of the structure. Numerical simulations reveal that SPH is actually capable of correctly replicating the structural deformations even for low mesh refinement. On the other hand a low refinement gives a poor approximation of the pressure distribution over the fluid/structure interface. However, this lack of accuracy seems to have negligible effect on the structural deformation.

Being able to model the fluid with a low mesh refinement means lower computational time which is, from the practical point of view, the most delicate point for the applicability of the SPH technique to full-scale three-dimensional simulations to be used for design purposes.

2 Experimental Set-Up

As shown in the previous sections, hydroelasticity in water-entry problems has been studied by many authors, both by experimental campaigns and by numerical simulations (e.g. [16,24,26,27,48]). However, their interest mostly focused on the analysis of the pressure at the fluid/structure interface rather than the structural deformation itself. Furthermore, all the structures used in the experiments are stiff and present very little structural deformation. Consequently, hydroelastic effects are low.

Instead, the experimental part of this work is not focusing on the impact pressure but on the structural deformation itself. An experimental apparatus was designed to perform slamming tests of wedges of various stiffness and to compare them with the theoretical results shown in the previous sections and numerical simulations. The time history of the hydrodynamic force applied on the wedge and the strains at several locations on the panel are measured. The design of the testing machine and the specimens was chosen in order to avoid air trapping effects, as described in Sect. 1.3.

2.1 Description of Models and Tests

A drop weight machine (Fig. 3) with a maximum drop height of 4.5 m was specially designed and built. The machine is composed by an aluminum frame 2 m long, 1.8 m wide and 6 m high, holding two prismatic rails guiding an aluminum sledge (Fig. 4). The rails have a maximum vertical run of 4.0 m so that the wedge can fall from various heights leading to different entry velocities. Teflon insets minimize the friction between the sledge and the prismatic rails. The sledge can hold wedges up to 350 mm long (per side) and 800 mm wide. The falling body hits the fluid at the center of a tank 1.2 m wide, 1.8 m long and 1.1 m deep. The tank was filled with

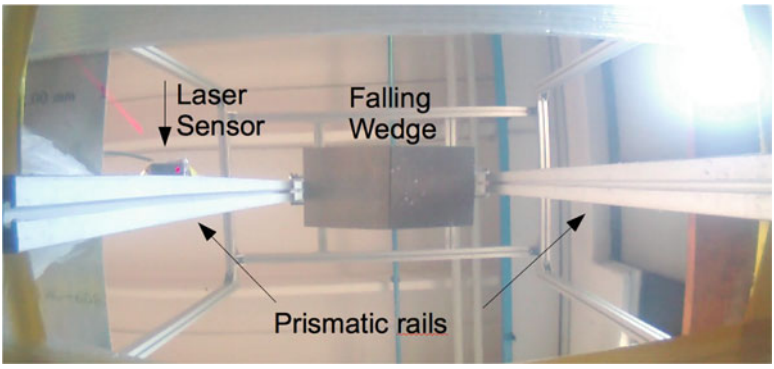

Fig. 3 Picture of the drop weight machine seen from the *bottom* of the water tank

Fig. 4 Picture of the sledge with an aluminum wedge mounted on it

water only up to 0.6 m to prevent the water waves generated during the impact to overflow. The drop heights, which are defined as the distance between the keel and the water surface, ranged from 0.5 to 3 m at 0.25 m increments.

Impact acceleration is measured by a *V-Link Microsrain* wireless accelerometer (± 100 g) located at the tip of the wedge. All reported accelerations are referenced to 0 g for the free-falling phase. The sampling frequency is set to its maximum of 4 kHz. Entering velocity is recorded by a laser sensor ($\mu\varepsilon$ ILS 1402) capturing the sledge position over 350 mm of ride at a frequency of 1.5 kHz with a definition of 0.2 mm. The entry velocity is obtained by the numerical differentiation of the position. The maximum impact height is 4 m, corresponding to a maximum impact velocity of 8.8 m/s. This maximum impact velocity cannot be reached during experiments due to the large wedge dimensions offering a high air resistance. Friction on the prismatic rails was found to be negligible compared to the air resistance.

One of the main requirements was to be able to easily test a high number of wedges with different stiffness and deadrise angle without having a large number of specimens. Thus, wedges were designed to be composed of two panels (Fig. 5) joined together on one side (keel) by a mechanism capable to change the deadrise angle smoothly from 0° to 50°. The impact angles were measured at rest with a digital level providing 0.1° resolution. Figure 6 shows a conceptual sketch of the wedge.

In nautical applications, composite hulls are usually made by panels whose edges are clamped to the main frame (a sketch of this configuration can be seen in Fig. 7). Locking all the edges of the panel has the effect of increasing the first natural frequency. However, the literature [16, 22–27] indicates that hydroelastic

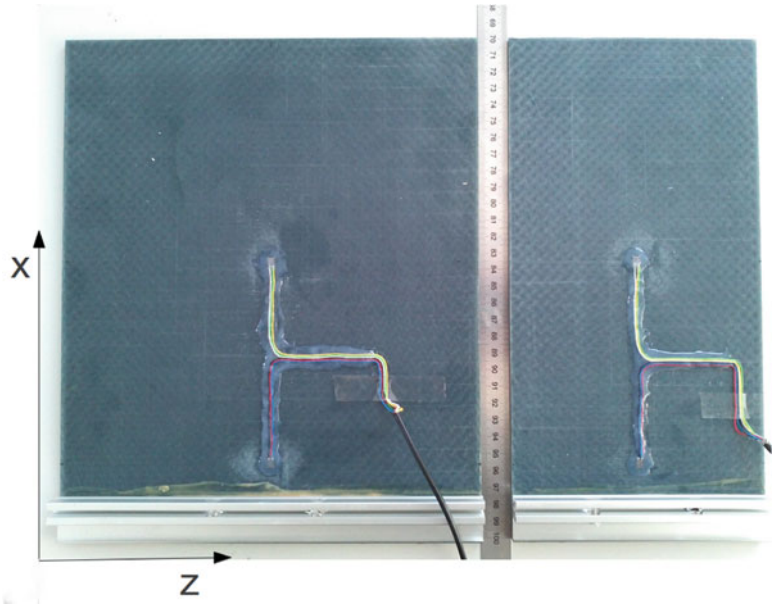

Fig. 5 Picture of two composite panels of different width: 250 and 150 mm

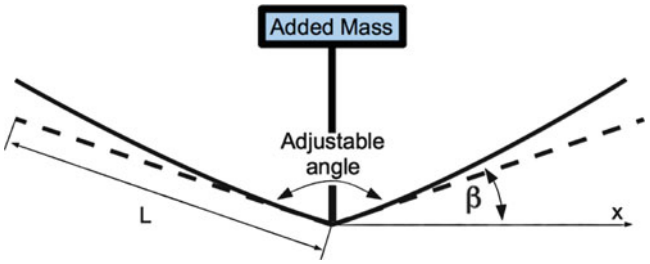

Fig. 6 Conceptual scheme of the wedge used for experiments. L panel length. β deadrise angle. *Dashed line*: undeformed panels, *solid line*: expected deformation during impact

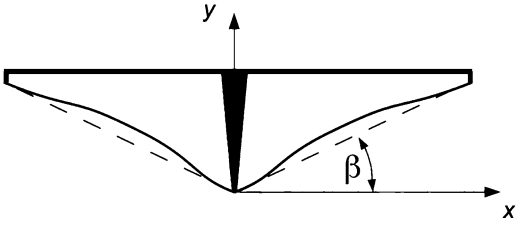

Fig. 7 Sketch of a wedge clamped on two sides. *Dashed line*: initial configuration, *solid line*: expected deformation during impact

effects increase while increasing the entry velocity and decreasing the ratio between the wetting time and the first natural frequency. This means that hydroelasticity is more likely to appear for structures having longer natural period. Consequently hydroelastic effects appear at lower impact velocity in case of flexible structures

Table 1 Plates material properties

Material	Abbr.	$E_1 = E_2$ (GPa)	ν_{12}	ρ(kg/m^3)
6068 T6	A	68	0.32	2,700
E-Glass (mat)/vinylester	V	20.4	0.28	2,050
E-Glass (woven)/epoxy	W	30.3	0.28	2,015

Table 2 First three dry natural frequencies of the panels used for experiments

Abbr.	Material	Thickness (mm)	$\omega_1, \omega_2, \omega_3$ (Hz)
A2	Aluminum	2	18.01 112.89 316.12
A4	Aluminum	4	36.03 225.79 632.24
V2	Fibreglass	2.0	9.77 61.22 171.44
V4	Fibreglass	4.0	19.73 123.67 346.29
W2	Fibreglass	2.2	19.69 123.40 345.54
W4	Fibreglass	4.4	37.80 236.94 663.44

than for stiff structures. From the experimental point of view there are two main advantages when using wedges with a longer first natural period:

- Experiments can be conduced at lower velocities
- Deformations are larger and consequently easier to measure

For these reasons, wedges are designed as two panels rigidly connected only at the keel edge. All the others edges are free to deform.

2.2 Specimens

Ref. [16] shows that hydroelasticity is influenced by the ratio between the wetting time and the panel's lower natural frequency. To vary the fundamental natural frequency of the panels, different stiffness to area density ratios are needed. Thus, aluminum (A), E-glass (mat)/vinylester (V) and E-Glass (woven)/epoxy (W) panels of various thickness (2 and 4 mm) were used. All wedges are made by two panels 300 mm long, but with two different width: 150 and 250 mm. Aluminum and Composite panels material properties are listed in Table 1. Composite panels were produced by VARTM by infusion of vinylester resin on E-Glass fibre mat, while the E-glass (woven 0°/90°)/epoxy panels were produced in autoclave.

All panels were equipped with two strain gauges per side, located at 25 and 120 mm from the reinforced tip, as shown in Fig. 5. The reinforced tip is 27 mm long and is used to connect the two panels to the aluminum sledge.

The position of the strain gauges was chosen on the basis of a dry modal analysis: they were placed far from the nodes (referred to the deformation) of the first three mode shapes, whose frequencies are listed in Table 2. Note that the nodal position referred to the strains are not the same one of the modal shapes, as visible in Fig. 8.

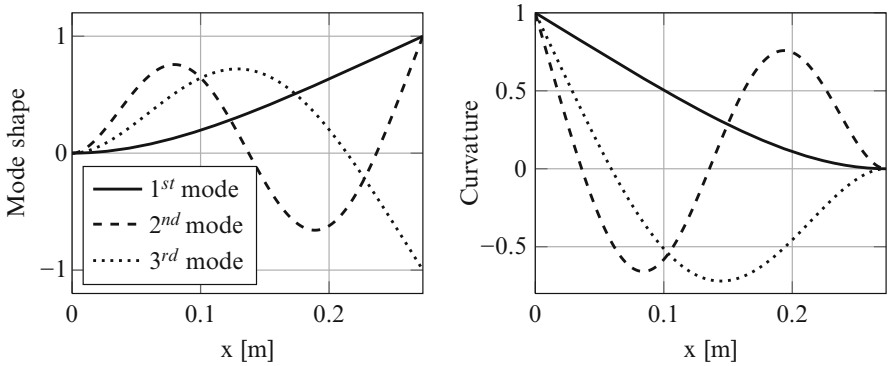

Fig. 8 Mode shapes of a dry panel (*left*) and curvature (*right*). The comparison of the two graphs shows that the position of the nodes is different. The location of the strain gauges was chosen as 25 and 120 mm from the clamped side

3 Experimental Results

For each combination of material, plate thickness, impact height and deadrise angle, experiments were repeated three times to guarantee the accuracy of the measures and to verify the repeatability of the tests. A total of more than 1,200 experiments have been conducted, only a few of these results are presented in this work. Figures 9 and 10 show the impact-induced deformations of composite wedge (W2) with deadrise angle of 30° entering the water at 2.77 and 6.28 m/s respectively. Each test case was repeated three times, showing a very good repeatability.

The response of the wedges in terms of structural deformation show different behavior varying the impact parameters: entry velocity, deadrise angle and stiffness to area mass ratio. In Fig. 9 the signals of the two strain gauges show smooth shape and their trend is similar, suggesting that the first mode of vibration dominates the structural deformation. A different behavior is recorded when the impact velocity is higher (Fig. 10), where the deformation recorded by the strain gauges located at the center of the plate follows the overall trend recorded by the first strain gauge but marked oscillations appears, suggesting that more than one mode shape is excited. Furthermore, it was observed that the maximum strain is not always recorded by the strain gauge located at 25 mm from the wedge tip, but for the most severe impacts (higher velocity and lower deadrise angle) the maximum value is recorded by the strain gauge located at 120 mm from the wedge tip. Figure 11 show the results of a composite wedge (W2) with deadrise angle of 30° entering the water with various impact velocities. Recorded accelerations show good repeatability. The scatter on the maximum acceleration recorded during the three repetitions is below $\pm g$ for all the impact cases.

Experiments show that the structural flexibility affects the acceleration during the water entry. It was found that: if the structural deflection is small, this has

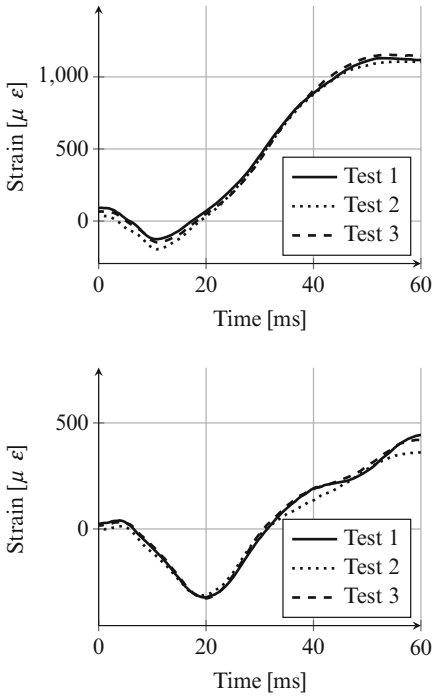

Fig. 9 Example of a composite (W2) wedge, 2 mm thick, $\beta = 30°$, $V_0 = 2.77$ m/s. Strain recorded at 25 mm (*top*) and 120 mm (*bottom*) from the wedge tip. Three repetitions of each impact case are shown, revealing extremely good repeatability

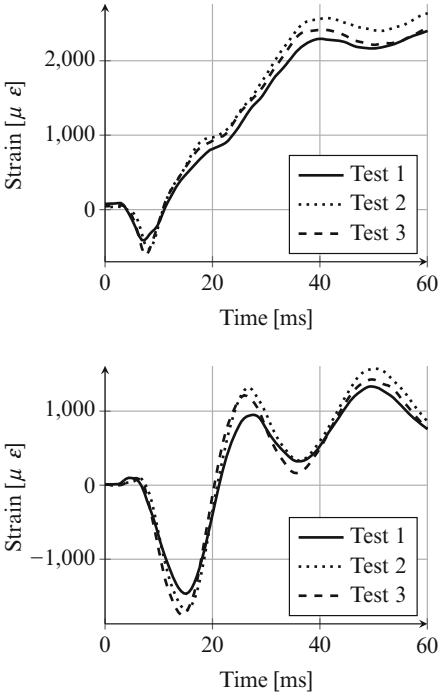

Fig. 10 Example of a composite (W2) wedge, 2 mm thick, $\beta = 30°$, $V_0 = 6.28$ m/s. Strain recorded at 25 mm (*top*) and 120 mm (*bottom*) from the wedge tip. Three repetitions of each impact case are shown, revealing extremely good repeatability

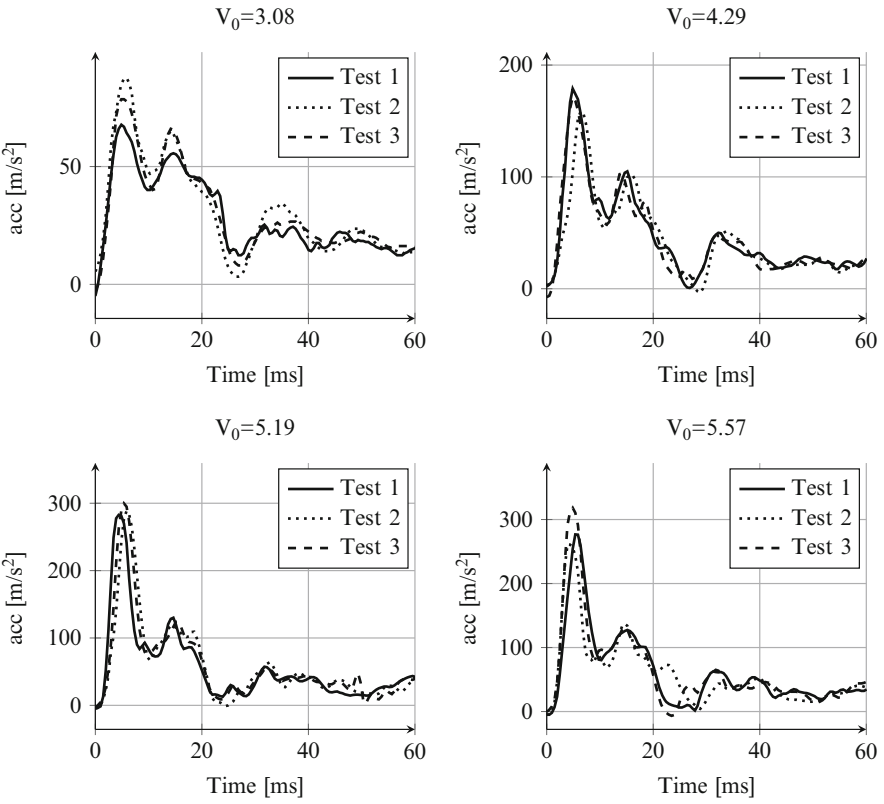

Fig. 11 Accelerations during the water entry of a wedge (W2) with deadrise angle $\beta = 30°$ entering the water at various impact velocities. Three repetitions of each impact case are shown, revealing extremely good repeatability

very little influence on the accelerations. While, if the structural deflection is high, accelerations show high oscillations if compared to to the water entry of a rigid body. As examples, Figs. 12 and 13 show the comparison between the solution for a rigid wedge (blue line) and the recorded accelerations of flexible wedges (black lines). The structural deformation is increasing as the impact velocity increases (left to right, top to bottom in the Figures) and as the deadrise angle decreases (the deadrise angle is reducing from Figs. 12 to 13). Looking the graphs in this order is evident that there is an increase of the oscillations in the accelerations as the structural deformation increases. Furthermore, while for low entry velocities and high deadrise angles the maximum acceleration is the same one as for the rigid case and the acceleration oscillations are low; as these oscillations increase, the maximum acceleration and the time this is reached moves from the rigid-body solution. In particular, the maximum acceleration lowers compared to the one experienced by rigid bodies.

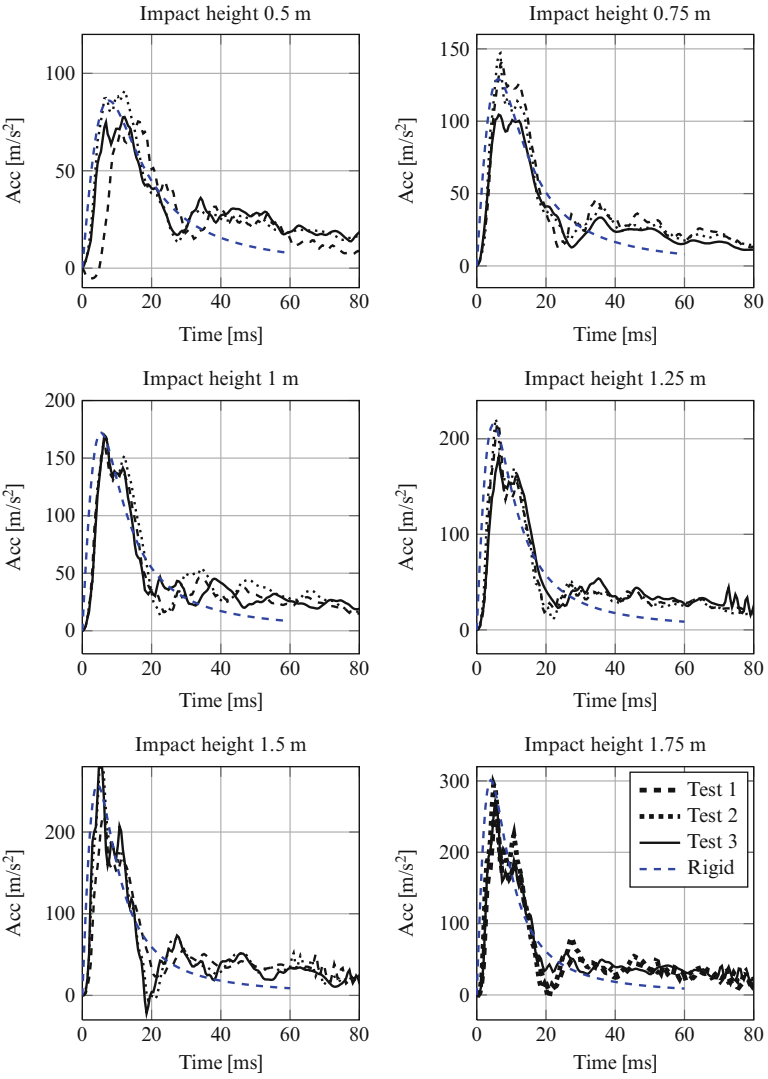

Fig. 12 Recorded accelerations of a composite wedge with $\beta = 25°$ impacting from various impact heights (three tests for each configuration, *black lines*) compared with the acceleration of a rigid wedge (*blue line*)

A secondary effect of hydroelasticity can be appreciated in the next graphs: Fig. 14 shows the recorded strains for a composite wedge (V2) with given deadrise angle presented as function of the drop height, while Fig. 15 shows the recorded strains for an aluminum wedge 2 mm thick presented as function of the deadrise angle for a given impact velocity. Figure 15 shows that the deformation in time is very smooth when the velocity is small (left plot on top), while the dynamic

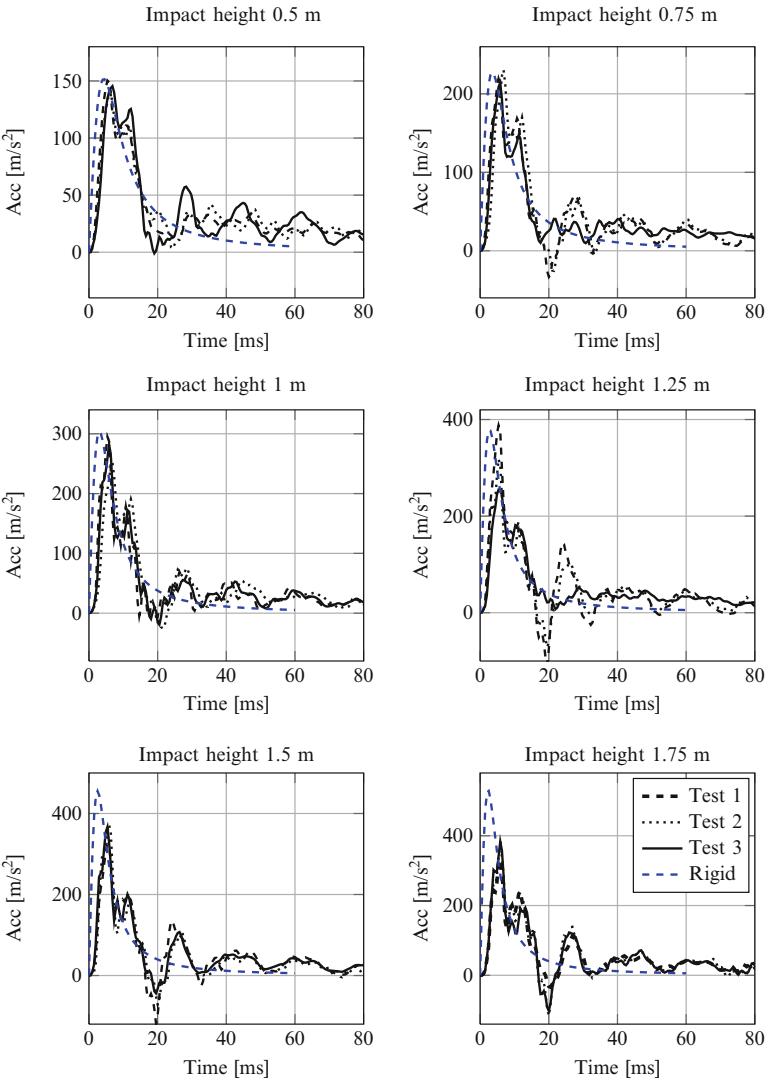

Fig. 13 Recorded accelerations of a composite wedge with $\beta = 15°$ impacting from various impact heights (three tests for each configuration, *black lines*) compared with the acceleration of a rigid wedge (*blue line*). An increasing dynamic response is clearly visible as the impact speed increases

response increases as the impact becomes more severe. The fourth plot (bottom, right) clearly shows this transition: the wedge with higher deadrise angle (35°, black full line) shows a smooth (almost sinusoidal) response; as the deadrise angle decreases oscillations appears. These results show that, as the impact becomes more severe, the dynamic response switches from a single-mode dominated response to a multiple-mode dominated deformation.

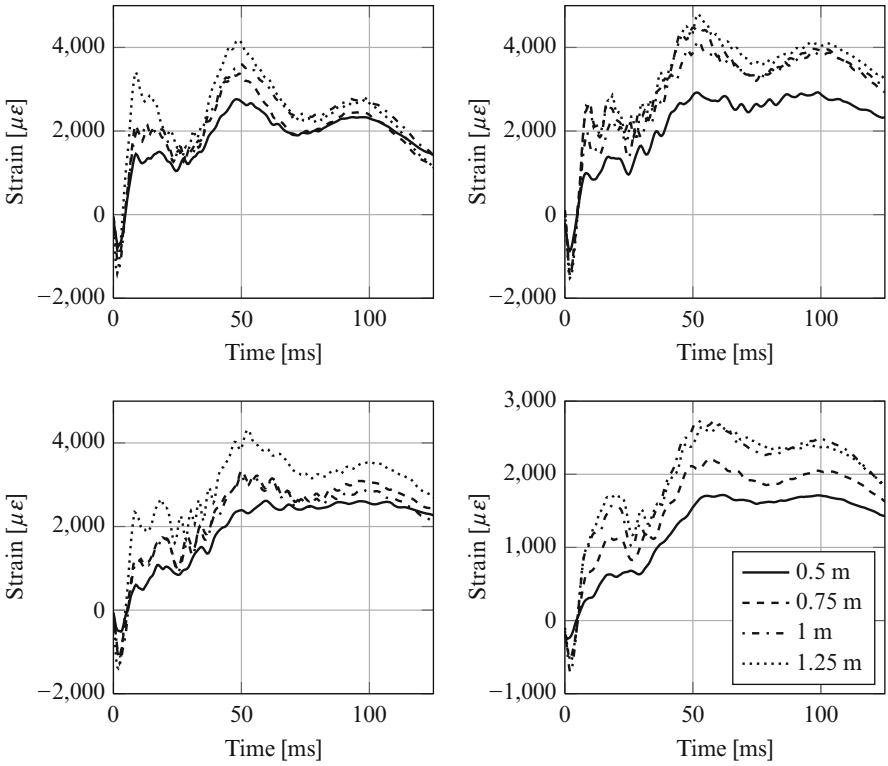

Fig. 14 Experimental recorded strains for various drop heights. Composite panel (V2), 2 mm thick. $\beta = 10^\circ$ (*top*, *left*), $\beta = 15^\circ$ (*top*, *right*), $\beta = 20^\circ$ (*bottom*, *left*), $\beta = 25^\circ$ (*bottom*, *right*)

Experiments show that in all the impact cases the strain measured by the strain gauge closer to the wedge apex initially assumes negative values. The strain is associated to the local curvature of the wedge, revealing that the panels are deforming downward at the very beginning of the impact. This deformation is opposite to the one induced by the impact pressure, that is pushing the wedge to deform upwards. This initial negative deformation has to be attributed to the effect of inertia: the hydrodynamic load acts on the wedge apex at first, to later spam on a larger area as the wedge enters the water. Furthermore, the maximum impact load is reached close to the beginning of the impact and rapidly decreases. Consequently, at first deformations are induced by the inertia of the panels that are being decelerated during the impact and consequently deform downward. As the wedge enters the water the hydrodynamic load covers a larger area and the deformation due to the pressure exceeds the deformation due to inertia, leading the strains to positive values.

Faltinsen [50] shows that, for local slamming-induced stresses, hydroelastic effects increase with decreasing deadrise angle β and increasing impact velocity V. Following a similar approach, we define a parameter R as the ratio between the

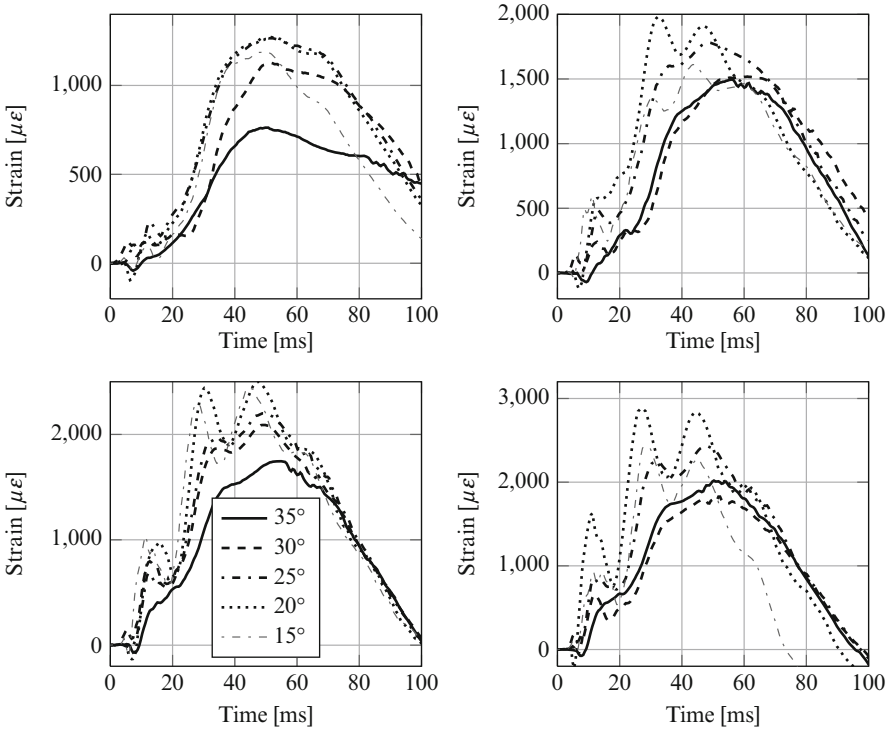

Fig. 15 Experimental recorded strains for various deadrise angle. Aluminium panel (A2), 2 mm thick. $V_0 = 3$ m/s (*top*, *left*), $V_0 = 4.2$ m/s (*top*, *right*), $V_0 = 5.2$ m/s (*bottom*, *left*), $V_0 = 6$ m/s (*bottom*, *right*)

wetting time and the lower natural period of the panel, where the wetting time was calculated by Wagner's approach. Figure 16 shows the non-dimensional recorded maximum strain $\frac{\epsilon_m EI tan(\beta)}{z_a V^2 \rho L^2}$ (as suggested in [50]) versus the parameter R. Where EI is the bending stiffness, z_a is the thickness and L is the panel length. Results of 2 mm thick panels are presented for various impact velocity, deadrise angle and material (blue marks: aluminum panels, red marks: composite panels (V), black marks: composite panels (W)). The non dimensional stress shows an increasing trend as the parameter R increases, to flatten once it reaches the unity value. This shows that hydroelastic effects (for the particular geometry studied) become important when the parameter R, which is proportional to the ratio between the wetting time and the first structural natural period, is lower than 1. In fact, in the range of $0 < R < 1$ the maximum strain is not proportional to V^2, as in quasi-steady-pressure loading, but decreases as the parameter R decreases. These results are similar to the one found by Faltinsen [16], whose model is based on the assumption of constant impact velocity and was not supported by experimental results.

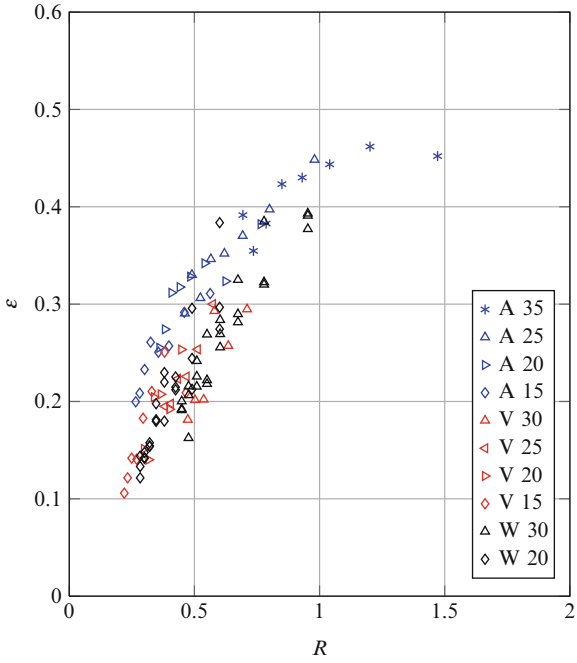

Fig. 16 Non-dimensional recorded maximum strain ϵ, presented as a function of a parameter R that is proportional to the ratio between the wetting time of a rigid wedge and the dry natural period of the panel [49]

4 Smoothed Particle Hydrodynamics (SPH)

A coupled FEM and SPH formulation available in the commercial FE code LS-Dyna was used to model the water entry of elastic wedges. In the following it is shown how the fluid is modeled and the validation of the SPH method to correctly study water entry problems. First, the SPH model is validated and optimized by comparison with analytical and numerical examples of simple problems. Then, the optimized model is used to study water impacts of elastic structures, comparing the numerical results with experiments.

4.1 Equation of State

To model the fluid, an equation of state (EOS) needs to be defined in LS-Dyna. In the literature the most used EOS is the Gruneisen model [51–53], which follows the formula:

$$p = \frac{\rho C^2 \mu \left[1 + \left(1 - \frac{\gamma_0}{2}\right)\mu - \frac{a}{2}\mu^2\right]}{\left[1 - (S_1 - 1)\mu - S_2 \frac{\mu^2}{\mu+1} - S_3 \frac{\mu^3}{(\mu+1)^2}\right]^2} + (\gamma_0 + a\mu)E \tag{13}$$

Table 3 Gruneisen model constants for water

C (m/s)	S_1	S_2	S_3	ρ (kg/m^3)	γ	a	E
1,480	2.56	1.986	1.2268	1,000	0.5	0	0

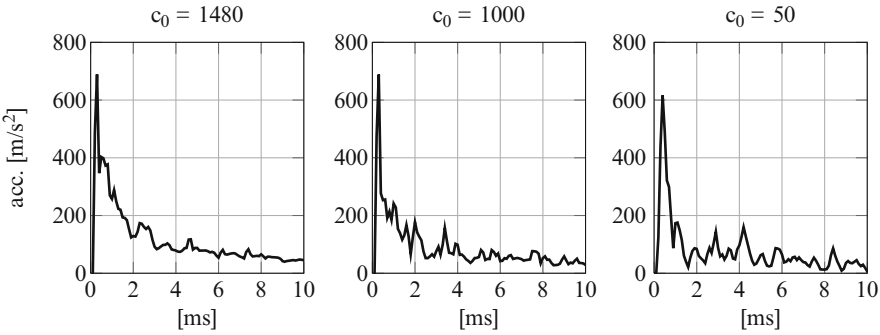

Fig. 17 Acceleration response of a wedge entering the water varying the bulk speed of sound. The acceleration shows increasing oscillations as the bulk speed decreases (*left* to *right*)

Where $\mu = \eta - 1$ (η is the ratio between initial an final density), C is the bulk speed of sound, ρ is the density of the fluid. There are many combinations for the constant that satisfy the water behavior. In this work we used the values presented in Table 3; values are taken from the literature [53].

By lowering the value of C it is possible to reduce the bulk speed of sound. A reduction in the pressure waves speed leads to an increase of the minimum time step needed for the solution and the consequent reduction of the computational time. Furthermore the traveling pressure waves take longer to reach the boundaries and reflect back towards the impactor, it is than possible to build a model where there are no reflected pressure waves during the entire solution time. A common value used in the literature for the waves speed is 80 m/s. The main disadvantage of this artifice is that, in case of slamming event, the quality of the impact dynamics get worse in terms of smoothness of acceleration and of the pressure distribution at the fluid/structure interface. For example, Fig. 17 shows the acceleration of a wedge entering the water at 4 m/s varying the bulk speed of sound (1,480, 1,000 and 80 m/s). Moving from the left graph to the right, as the bulk speed of sound decreases, the acceleration shows increasing oscillations.

To avoid this loss of quality it is necessary to increase the number of elements, increasing the computational time. For these reasons we preferred to use the real pressure wave speed of 1,480 m/s.

4.2 Validation of the Numerical Model

The numerical model should be capable of correctly predicting the fluid motion in order to replicate the impact dynamics of a body entering the water. At the same

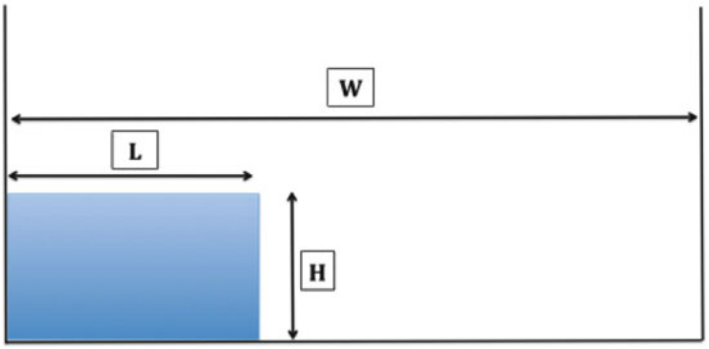

Fig. 18 Dam-break geometry. The *blue* region is the fluid, initially at rest, whose right boundary is suddenly removed to let the water occupy a larger tank. H = initial water depth, L = initial water length, W = water tank length once the boundary is removed

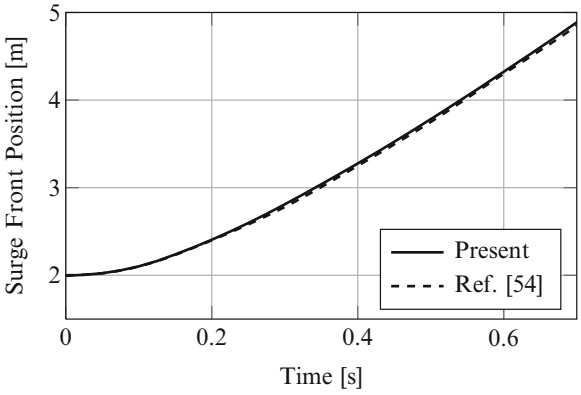

Fig. 19 Numerical solution of the surge front position vs. time. *Full line*: present solution. *Dashed line*: example from the literature [54]

time, the pressure distribution in the fluid should be accurate to guarantee the correct evaluation of the pressure at the fluid/structure interface. This section shows two models used to validate the numerical solution: the dam-break problem is used to validate its capability to treat the overall fluid motion, while the example of a water column subjected to a step load is used to evaluate the accuracy of the model when focusing on the pressure waves propagation.

The so called dam-break problem is often used in the literature as benchmark test to evaluate SPH accuracy ([40, 54–57]) in a two dimensional simulation of a water tank where a boundary is removed instantaneously to let the water to cover a larger tank (Fig. 18) where $f = 5.4\,\text{m}$, $L = 2\,\text{m}$ and $H = 1\,\text{m}$. The fluid is modeled by 180,000 particles and only the gravitational force is applied. Figure 19 shows the position of the front wave during time. Results about the water shape and the position of the surge front are in good agreement with those presented in the literature [40, 54–57]. However, while SPH seems to give accurate results for

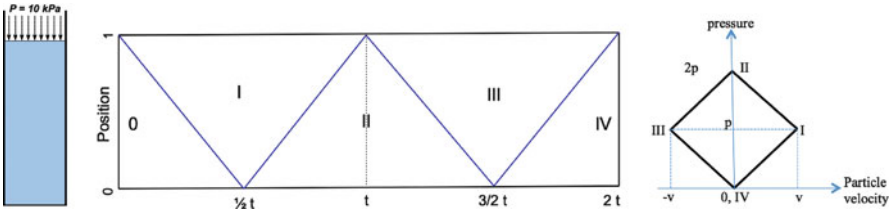

Fig. 20 *Left*: sketch of the water column loaded at the free surface by a constant pressure. *Center* and *right*: Lagrange diagram. Analytical solution for the reflection of a pressure wave during time

particles velocity and water flow, it seems not to correctly account for the pressure field, as it will be shown in the next example. In fact, as other numerical methods, SPH suffers noise in the pressure evaluation due to numerical fluctuations, leading to a poor definition of the pressure at the fluid/structure interface. This behavior is well known in the literature [58] and much effort is being spent on it. The most used technique to suppress these pressure fluctuations is the introduction of an artificial viscosity. Most of the work found in the literature focuses on the suppression of pressure oscillations in gases and solids [59–61]. To take into account the artificial viscosity [58,62], an artificial viscous pressure term q is added such that the pressure p of the ith particle is computed as:

$$p_i = p_i + q \tag{14}$$

where

$$q = \beta \cdot \rho \cdot h_i \cdot \dot{\epsilon}_{kk}^2 - \alpha \cdot c_0 \cdot \dot{\epsilon}_{kk} \tag{15}$$

where h_i is the minimum distance between the particles, α and β are the linear and quadratic coefficients and $\dot{\epsilon}$ is the strain rate. For gases the linear and quadratic terms are usually in the range $\alpha = 1.0 \div 4.0$ and $\beta = 1.5 \div 2.0$, while for solids $\alpha = 0.06$ and $\beta = 1.5$.

To study the influence of the artificial viscosity term for liquids, numerical results have been compared with an example considering a water column suddenly subjected to a uniform pressure load equal to 10 kPa on the free surface. An analytical solution to this problem is found assuming that it is governed by the one dimensional wave equation. Boundaries are fixed. Figure 20 shows the Lagrange diagram, which is divided in five regions, namely 0, I, II, III and IV. In region 0 and IV the pressure is null, in region I and III the pressure equals the applied pulse and in region II the pressure is twice the applied pulse. The related stress history at the top, bottom and middle of the water column is presented in Fig. 21. At the top, the pressure remains constant and obviously equals the applied pressure. At the bottom, pressure is zero until the first pressure wave reaches the boundary at time $1/2t$, when the wave is entirely reflected and the pressure becomes twice the incident pulse. Once the reflected wave reaches the top, at the time t, a second pressure wave of intensity equal to the applied pressure, but negative, is generated.

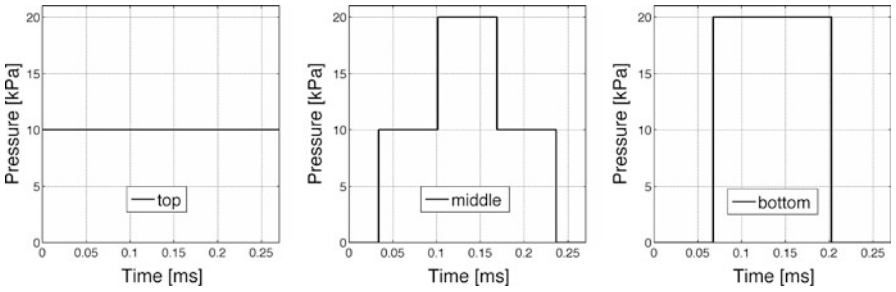

Fig. 21 Analytical solution of the pressure due to a wave propagation at the top (*left*), middle (*center*) and bottom (*right*) of a water column

This second wave reaches the bottom at time $3/2t$, it entirely reflects and the pressure at the bottom returns to zero. At the middle the pressure turns from zero to the applied pressure at time $t/4$, when the first wave pass through; the reflected wave arrives at time $3t/4$, switching the pressure to twice the applied pulse. The second (negative) wave arrives at $5t/4$, lowering the pressure again to the applied pressure, and the second reflected wave brings the pressure again to zero at time $7t/4$. In an ideal fluid this scheme continues infinitely with a period of $2t$.

Figure 22 shows the numerical results varying the linear bulk viscosity coefficient α of Eq. 15 (the quadratic term was found to have negligible effects) for a water column with particle spacing of 1 mm. The travelling wave theoretically switches the pressure value instantaneously without transitions. This behavior is difficult to reproduce numerically, since there is a transition between two different pressure regions which produces oscillations in the solution. This is known as Gibb's phenomenon and it occurs for most numerical methods unless some particular steps are taken to avoid it. These oscillations cannot be eliminated, but refining the particle size can reduce their duration and amplitude. The numerical results show that the artificial damping is effective for values as low as 0.2, and numerical fluctuations are entirely smoothed out for values of α greater than 0.5. These results show that the introduction of the artificial viscosity term lowers the pressure oscillations. However, in case of water-entry problems, the impact dynamics is negatively affected, as indicated by the results shown in Fig. 23. The graphs show the displacement and the velocity in time of a rigid wedge with a deadrise angle of 30° entering the water with an initial velocity of 4 m/s for various bulk artificial viscosity term. It is found that the higher the viscosity term, the higher the fluid resistance: the wedge decelerates more rapidly as the viscosity term increases, showing that α needs to be chosen as low as possible. For all the examples studied during this work α has been chosen to be lower than 0.2.

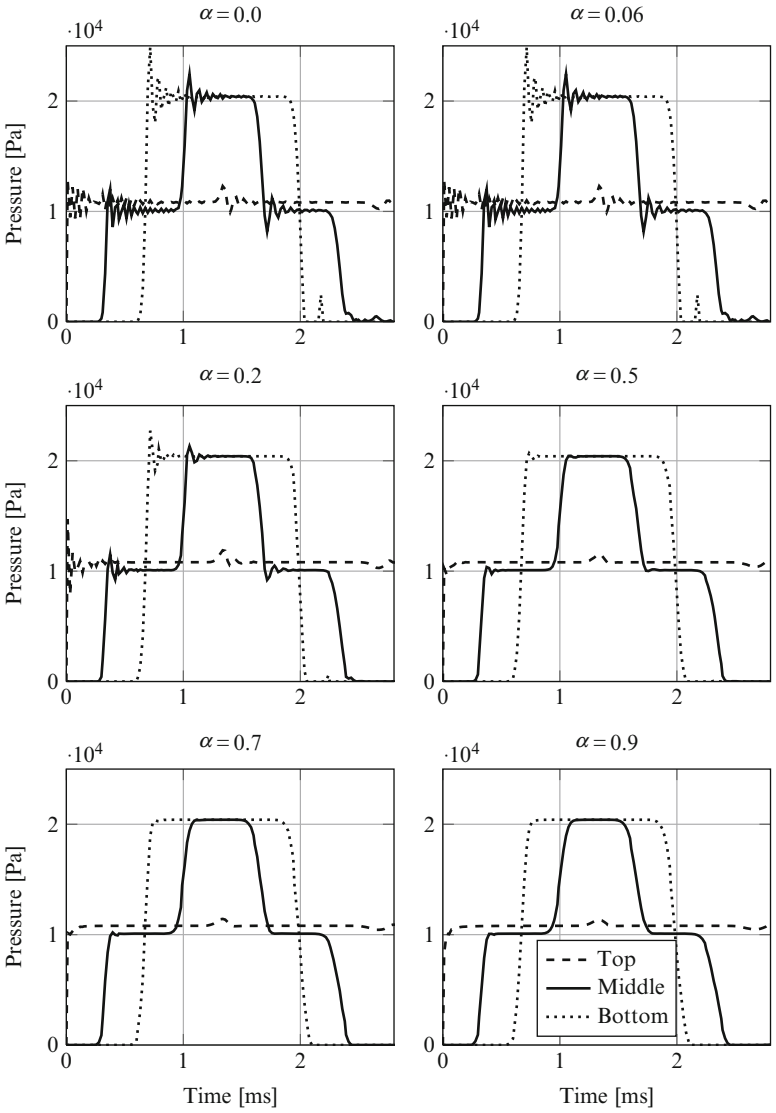

Fig. 22 Numerical pressure fluctuation reduction varying the linear artificial viscosity coefficient. *Dashed line*: top. *Full line*: middle. *Dotted line*: bottom of the water column

4.3 Non Reflecting Boundaries

In case of impacts on wide water surfaces, these can be considered as infinite since there are no reflected pressure waves travelling back to the impacting body. On the contrary, numerical solutions are necessarily affected by these reflected pressure

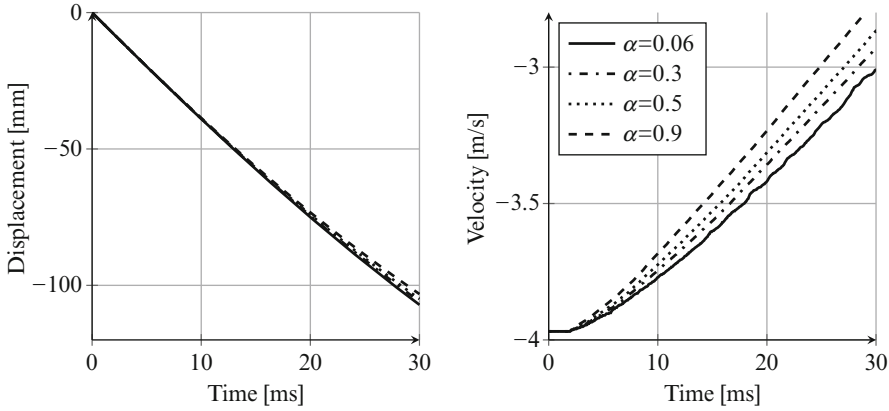

Fig. 23 Displacement and velocity during slamming of a rigid wedge entering the water with an initial velocity of 4 m/s varying the bulk artificial viscosity term α

waves, since to reduce the computational time it is necessary to limit the fluid domain. One of the most used technique to suppress the reflected pressure waves is to lower the speed of sound in the fluid (usually it is lowered from 1,480 to 80 m/s). As mentioned in Sect. 4.1, lowering the pressure waves speed permits to eliminate the reflected waves from the solution. However, since it is not always allowable to lower the sound speed, other techniques have to be used. In [63] Gong et al. proposed an improved boundary treatment capable to suppress wave reflection. They modeled the fluid with its real properties except for the last particles close to the boundary limits, whose sound speed has been reduced. This method presents the advantage of modeling the right fluid behavior together with the capability to entirely suppress the reflected pressure waves. Figure 24 shows the effect of the non reflecting boundaries in the case of a wave generated by the water entry of a cylinder: the pictures on top show a cylindrical pressure wave moving from the top to the bottom that, after 2 ms, is reflected in the case of rigid boundaries (on the right), while the non-reflcting boundaries (on the left) entirely absorbed it.

4.4 Comparison with Analytical Models

The optimized SPH model is now used to study the water entry of rigid wedges and its results are compared with those from the analytical models presented in Sect. 1.1. The model of the water entry of the wedge is based on the following main assumptions:

1. The fluid free surface is initially at rest;
2. Air is not included in the model. Air cushioning and air entrapment are consequently neglected;

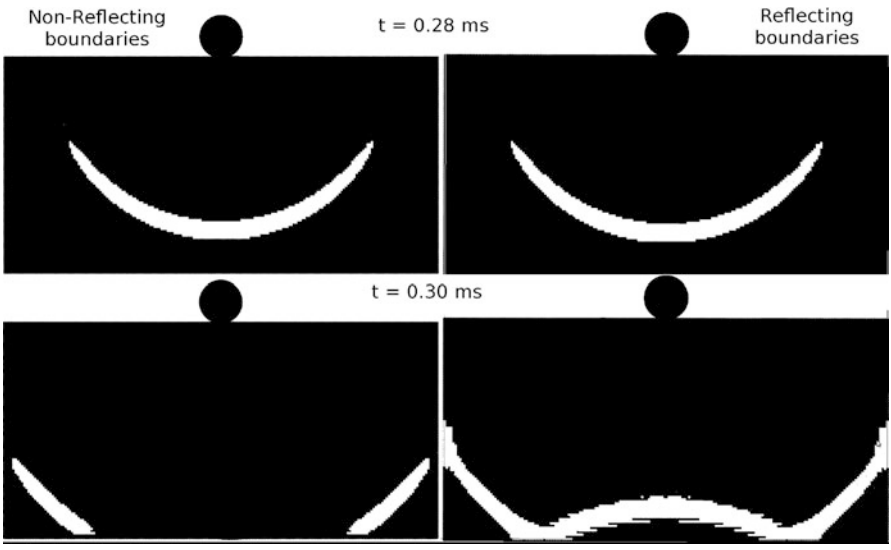

Fig. 24 Position of a pressure wave generated by the water entry of a cylinder before and after it reaches the boundaries: non-reflecting boundaries (*left*, the wave is absorbed) vs. rigid boundaries (*right*, the wave is reflected)

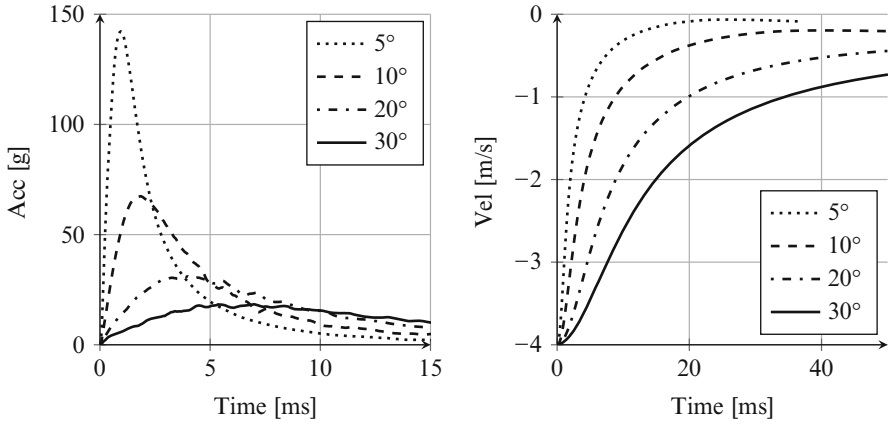

Fig. 25 Acceleration and velocity of a wedge varying the deadrise angle β. Total wedge mass: 20 kg per unit width. SPH simulations with rigid wedges

3. The wedge is assumed infinite along the z-axis (3D boundary effects are not included);
4. The problem is symmetrical with respect to the zy plane (y is the gravity direction, as in Fig. 6).

Figure 25 shows the SPH numerical results of the impact dynamics for rigid wedges of various deadrise angle entering the water at 4 m/s. The numerical results show a

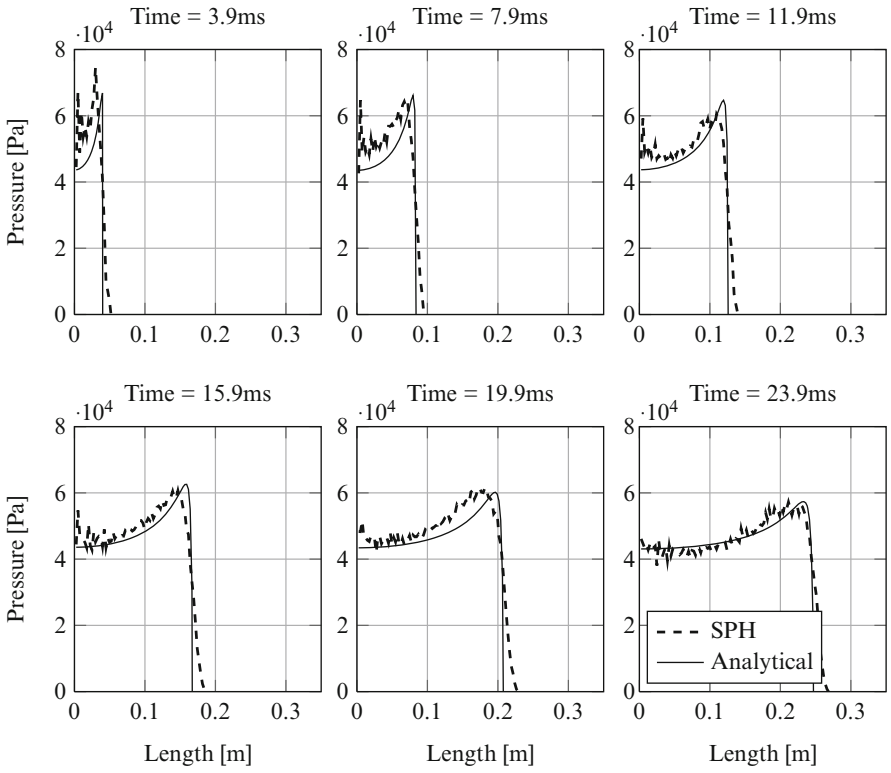

Fig. 26 Pressure in time at the fluid/structure interface for a wedge of 500 kg/m, deadrise angle 30° and initial velocity $V_0 = 4$ m/s. *Full line*: Wagner analytical solution. *Dashed line*: numerical results

good agreement with Von Karman's solution (Fig. 2) and Eqs. 2–6. The difference between the analytical and the numerical maximum impact force is always lower than 5% while the difference between the time the force peak is reached is lower than 15%.

Figure 26 shows the comparison of the pressure along the wedge between Wagner's solution and the numerical results for a wedge entering the water at 4 m/s with a deadrise angle of 30° and a mass per unit width of 500 kg/m. SPH results are in very good agreement with Wagner's solution except for the very initial contact time, since there are too few elements in contact to show a smooth pressure distribution at the interface. The maximum pressure value is reached at the beginning of the impact, and is constant for a given entry velocity and deadrise angle, while mass is affecting only the impact dynamics.

These results validate the SPH method and reveal that it is actually capable of predicting the impact dynamics and the pressure at the fluid/structure interface of rigid bodies entering the water. Thus, the SPH method will now be used for the analysis of water impacts of elastic structures, where analytical solutions are not available.

Table 4 Scheme of numerical simulations. The table shows the abbreviation of the various combination of material, thickness and entry velocity

	Material	Thickness (mm)	Impact velocity (m/s)
A2-4	Aluminum	2	4
A4-4	Aluminum	4	4
A2-2	Aluminum	2	2
A4-2	Aluminum	4	2
V2-4	Fibreglass	2	4
V4-4	Fibreglass	4	4
V2-2	Fibreglass	2	2
V4-2	Fibreglass	4	2

5 Elastic Wedges

The previous sections show that SPH is capable of modeling the impact dynamic and the pressure at the fluid/structure interface during the water entry of rigid wedges. In the following, elastic wedges are considered. The structural deformation might change the motion of the fluid introducing the so-called hydroelastic effects, causing the impact dynamics to differ from that of rigid wedges.

This section presents a parametric analysis of hydroelastic impacts of elastic wedges entering the water varying wedge flexural stiffness, impact velocity, deadrise angle and SPH particles size. Wedges are modeled as an ideally elastic aluminum (E = 70 GPa, $\nu = 0.3$, $\rho = 2{,}700\,\text{kg/m}^3$), or as an ideally elastic fibreglass mat composite ($E_1 = E_2 = 20$ GPa, $\nu = 0.3$, $\rho = 2{,}050\,\text{kg/m}^3$). To be able to compare wedges of different thickness, an added mass is applied to the tip of the wedge to reach a total mass of 20 kg per unit width in all analysis. Faltinsen [16] demonstrated that hydroelastic effects become important when

$$tan(\beta) \; < \; 0.25\, V \sqrt{\frac{\rho L^3}{E I}} \tag{16}$$

showing that the occurrence of hydroelastic effects depends on: impact velocity, deadrise angle and structural stiffness. In particular, the higher the impact velocity V, the lower the deadrise angle β and the higher the structure natural period T_1 is, the more important the hydroelastic effects are. To investigate the effect of hydroelasticity on the impact dynamics, wedges of different thickness were implemented: 2 and 4 mm, both for aluminum and fibreglass composite wedges. This way four different bending stiffness are considered: plates flexural stiffness compared to the stiffer one (aluminum 4 mm thick) are in the ratio of 1:1, 1:4, 1:8, 1:32. The effect of impact velocity has been also investigated. Table 4 shows the list of the numerical simulations campaign.

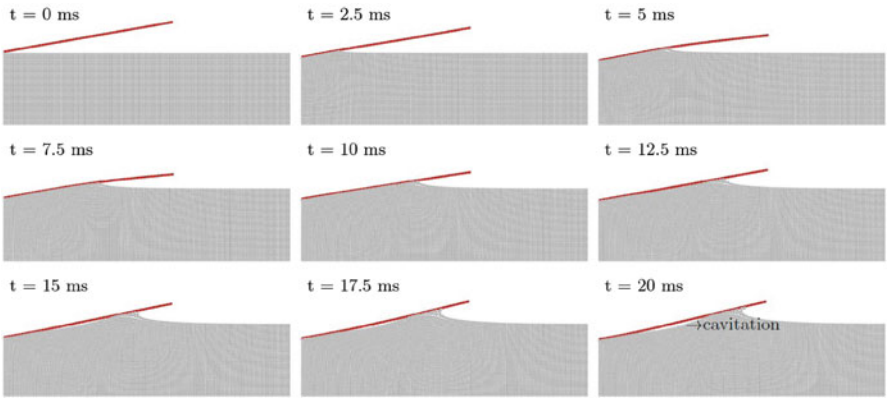

Fig. 27 Wedge deformation over time. 10° deadrise angle, 4 mm thick, 4 m/s initial velocity

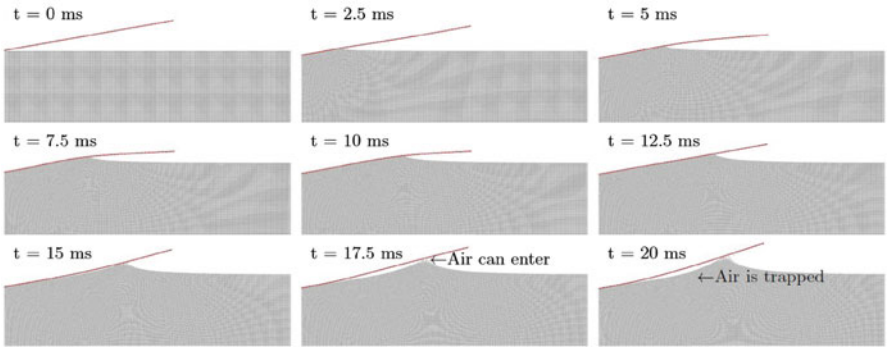

Fig. 28 Wedge deformation over time. 10° deadrise angle, 2 mm thick, 4 m/s initial velocity. Due to the structural vibrations some air might enter from the side and be trapped in the fluid

5.1 Hydroelastic Effects

Figures 27 and 28 show two examples of the water entry of deformable wedges. In the first one, an aluminum wedge 4 mm thick with deadrise angle of 10° is entering the water at 4 m/s. The second one shows the same example but the wedge thickness is 2 mm. Initially (up to 2.5 ms in these cases), the deformation of the wedge is low, so that it behaves like a rigid wedge. Then, the deformation of the wedge becomes important (≈5 ms) resulting into a mutual interaction between the fluid motion and the structural deformation. In this initial time of impact, the wedge is deforming downward due to its inertia. The wedge eventually reaches its maximum deformation (≈7.5 ms) and starts bending in the other direction (at ≈10 ms the wedge is in its neutral position, as shown in the central plot of Fig. 27). At this point, three events may happen:

1. The entire wetted portion of the wedge stays in contact with the water, and no air is entrapped in between the solid and the fluid. The fluid/structure interaction continues and the vibrations are damped by the fluid.
2. Along the wet part of the wedge the fluid tends to move away from the wedge, then pressure becomes negative and cavitation occurs, as shown in Fig. 27, from the seventh plot (when the impact time is 15 ms) and above.
3. The wedge detaches from the fluid and some air enters from the side. The air is eventually trapped in between the wedge and the fluid and an air cushion is generated, as shown in Fig. 28. In this case the interaction between the air flow and the fluid flow has to be taken into account.

In the cases studied, cavitation and ventilation phenomena appeared only in the cases of deadrise angle of 10° and initial velocity of 4 m/s (i.e. the most severe case). In all the other cases no fluid detachment was predicted.

An example of the effect of the structural deformation on the impact pressure in which no fluid detaches from the wedge and no air is trapped in the fluid during the impact is presented in Fig. 29. The plots show the comparison of the pressures over time of a rigid wedge vs. an elastic wedge (aluminum 2 mm thick) with deadrise angle of 30° and total mass of 20 kg/m entering the water at 4 m/s. It is found that the two solutions show extremely similar results at the beginning of the impact (until about 12 ms), when the impact pressure is higher. Pressures are similar until the panel has reached its maximum negative (leaded by the inertia) deformation. Once the wedge starts to deform in the opposite direction, the pressure eventually reduce to a lower value compared to the rigid case. Note that at this time the impact force is already in its descending phase and the maximum impact force has already been reached.

5.2 Impact Dynamics

This section presents a parametric study of the effect of fluid-structure interaction on the impact dynamics. Figures 30–32 show a parametric study varying the particle size of the numerical solutions of aluminum wedges 2 mm thick with deadrise angle of 10°, 20°, and 30° respectively, entering the water at 4 m/s. Since only vertical impacts are considered, one half of the wedge and water are modeled splitting the structure on its symmetry axis. Wedges side length is 300 mm while the fluid domain has been modeled as a tank 800 mm width and 600 mm height. Three particles sizes have been chosen for the simulations: 1 mm (*Fine model, 480,000 particles*), 2.5 mm (*Medium model, 192,000 particles*) and 5 mm (*Rough model, 48,000 particles*). The computation takes about 12 h to run in the case of fine model and only about 0.5 h for the rough model. Results show that the particle size is only slightly affecting the impact dynamics (velocity and acceleration are evaluated at the wedge tip). While velocity is computed correctly, the acceleration tends to present fluctuations increasing with the particle size, especially in the early stage of the impact. These

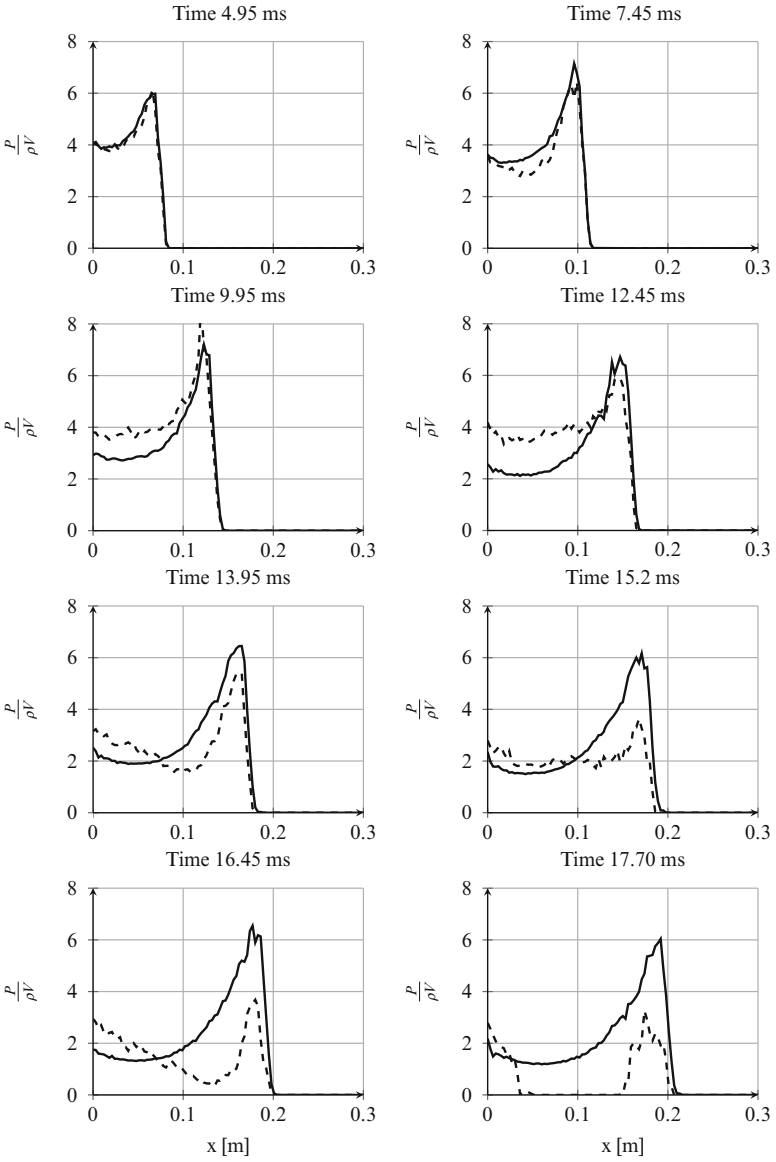

Fig. 29 Non-dimensional hydrodynamic pressure along the wedge over time. P is the hydrodynamic pressure, ρ is the density of the water and V is the instant velocity of the wedge. Deadrise angle 30°, mass 20 Kg/m. Comparison between rigid wedge (*solid line*) and elastic wedge (*dashed line*, aluminum wedge 2 mm thick). Results are similar at the beginning of the impact but diverges rapidly after 10 ms

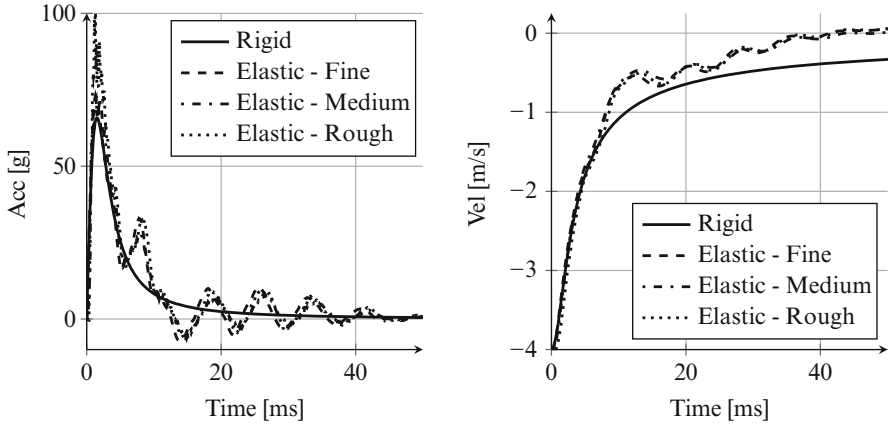

Fig. 30 Acceleration (*left*) and Velocity (*right*) of a wedge varying the particle size. Total wedge mass: 20 kg per unit width. Deadrise angle 10°. Comparison between the solution for a rigid wedge (*solid line*) and the simulation of a deformable wedge entering into a fluid modeled by three various particle sizes (*dashed lines*)

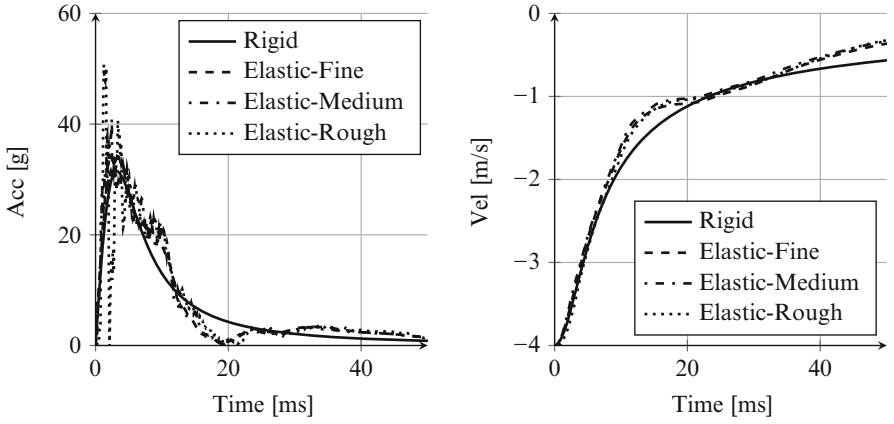

Fig. 31 Acceleration (*left*) and Velocity (*right*) of a wedge varying the particle refinement. Total wedge mass: 20 kg per unit width. Deadrise angle 20°. Comparison between the solution for a rigid wedge (*solid line*) and the simulation of a deformable wedge entering into a fluid modeled by three various particle sizes (*dashed lines*)

fluctuations increase with the deadrise angle. This behavior is due to the lower number of particles getting in contact with the wedge while raising the deadrise angle. Furthermore, the maximum acceleration is found to increase with the particle size due to the aforementioned fluctuations.

As expected from Faltinsen's [16] observations, the computed impact-induced acceleration are found to differ from the rigid case for all the deadrise angles investigated. Figures 30–32 show that the impact dynamic of the elastic wedges initially follows the solution for rigid structures until the maximum acceleration

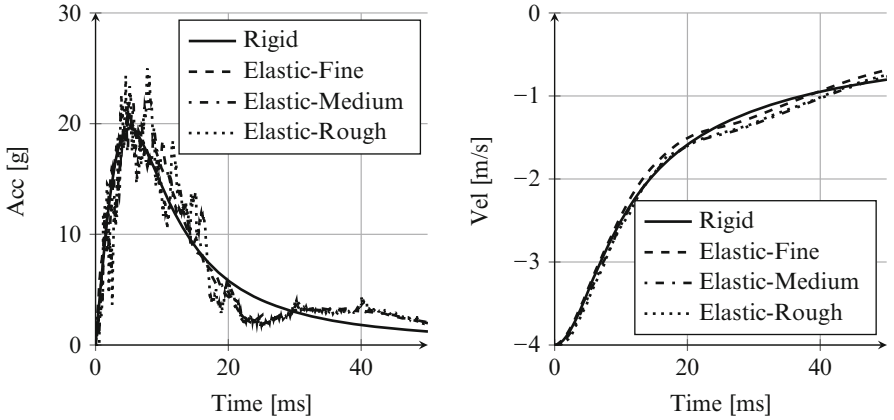

Fig. 32 Acceleration (*left*) and Velocity (*right*) of a wedge varying the particle refinement. Total wedge mass: 20 kg per unit width. Deadrise angle 30°. Comparison between the solution for a rigid wedge (*solid line*) and the simulation of a deformable wedge entering into a fluid modeled by three various particle sizes (*dashed lines*)

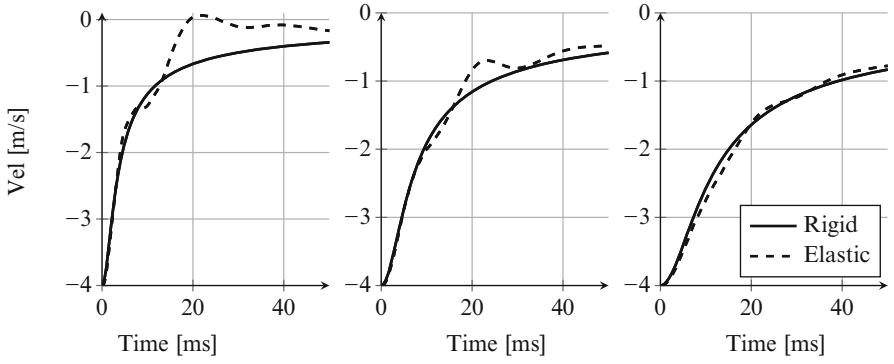

Fig. 33 Hydroelasticity effect on the impact dynamics of aluminum wedges 4 mm thick of different deadrise angles entering the water at 4 m/s. From *left* to *right*: 10°, 20°, 30° deadrise angle

is reached, to later differ due to oscillations whose magnitude increase as the maximum acceleration increases.

Figure 33 shows the comparison of the impact dynamics of elastic and rigid 4 mm thick aluminum wedges with different deadrise angles entering the water with an initial velocity of 4 m/s. As before, results are in accordance with Faltinsen's observations: hydroelasticity highly affects the impacts of wedges with deadrise angle from 5° to 20°, while the 30° behavior is close to the rigid wedge and very small hydroelastic effects appear. Figure 34 shows the same example but the wedges are entering the water at 2 m/s. In the cases of 20° and 30° deadrise angles fluid-structure interactions are small and elastic wedges behaves like the rigid wedges. Figures 35 and 36 compare the results for given deadrise angles and impact

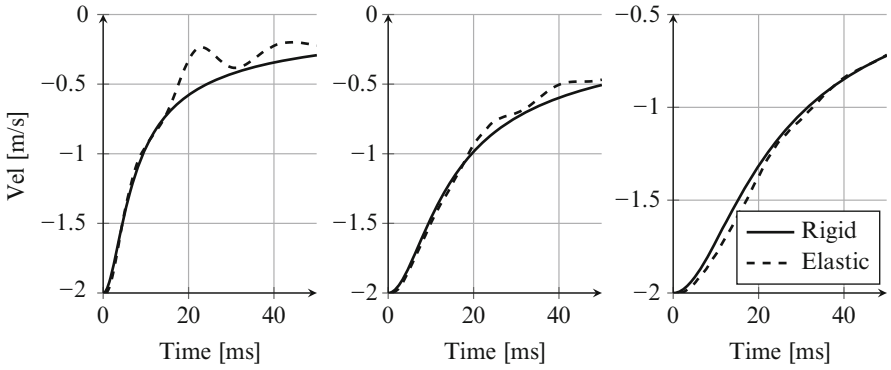

Fig. 34 Hydroelasticity effect on the impact dynamics of aluminum wedges 4 mm thick of different deadrise angles entering the water at 2 m/s. From *left* to *right*: 10°, 20°, 30° deadrise angle

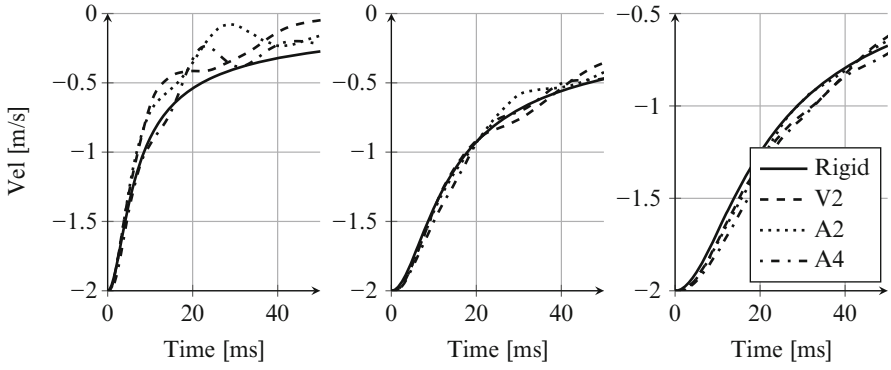

Fig. 35 Impact dynamics varying plate stiffness, deadrise angle from *left* to *right*: 10°, 20°, 30°, $V_0 = 2$ m/s

velocities varying the plate stiffness. Results are as expected: hydroelastic effects lower with increasing deadrise angles and plate stiffness, while they increase with the impact velocity. Further results about the importance of hydroelasticity on the structural deformation are presented in the next section, where a dependency of the structural response from the hydroelastic effect is shown.

5.3 Stresses Evaluation

It was shown in the previous section that increasing the particle size leads to an overestimation of the maximum acceleration due to oscillations in the computed acceleration, although the velocity is computed correctly. This section investigates the effect of the particle size on the stress computation.

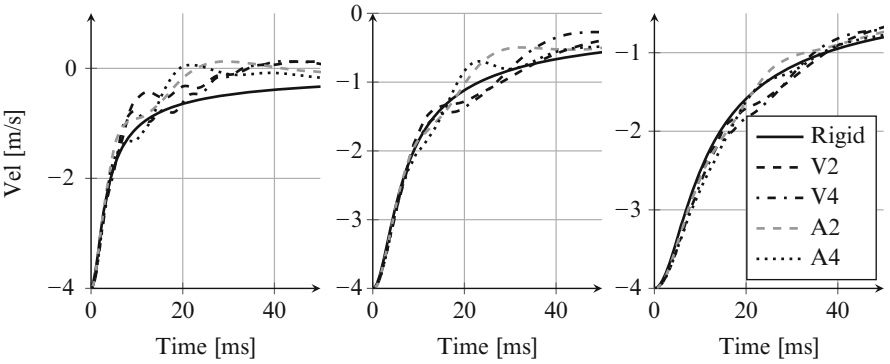

Fig. 36 Impact dynamics varying plate stiffness, deadrise angle from *left* to *right*: 10°, 20°, 30°, $V_0 = 4$ m/s

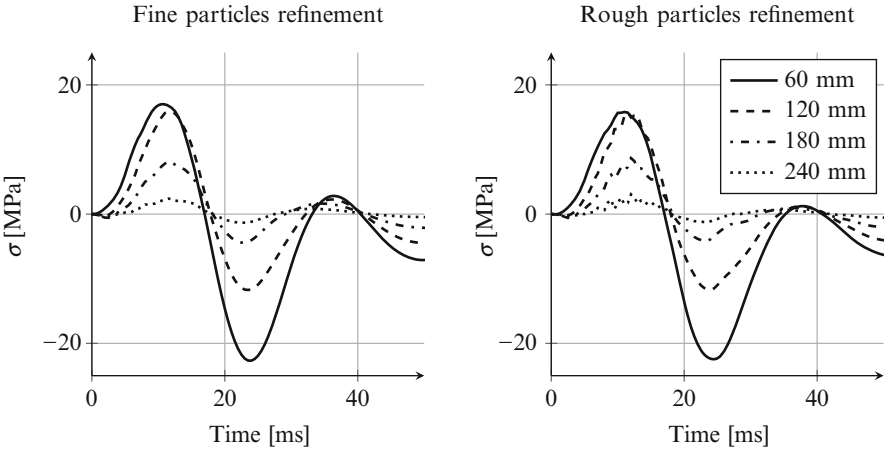

Fig. 37 Stresses at different distances from the wedge tip for fine and rough particle refinement. $\beta = 30°$, $V_0 = 4$ m/s

Figures 37 and 38 show the comparison of the stresses during time at different distances from the wedge tip in case of fine and rough particles refinement models. Results are definitely in good agreement, especially considering that the difference in the computational time between the fine particles model and the rough particles model is about 12 vs. 0.5 h. As mentioned before, the main disadvantage of increasing the particle size is that it becomes impossible to evaluate the pressure at the fluid/structure interface, however, this was found not to influence the evaluation of the structural deformation. The cases of 30° and 10° deadrise angles are shown, since these represent respectively the minimum and maximum influence of hydroelastic effects on the impact loads. In the first case, the wedge deformation is smooth with an almost sinusoidal shape, while moving to a more severe impact (lowering the deadrise angle from 30° to 10°) the stresses show high fluctuations, suggesting that more modes of vibrations superpose.

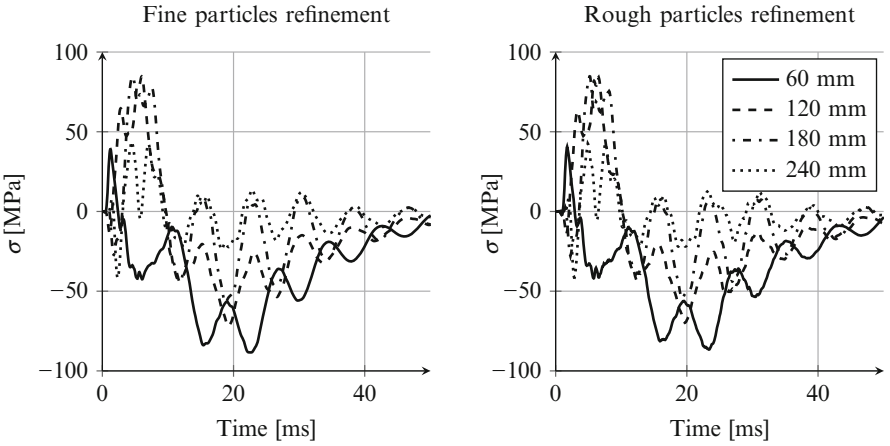

Fig. 38 Stresses at different distances from the wedge tip for fine and rough particle refinement. $\beta = 10°$, $V_0 = 4$ m/s

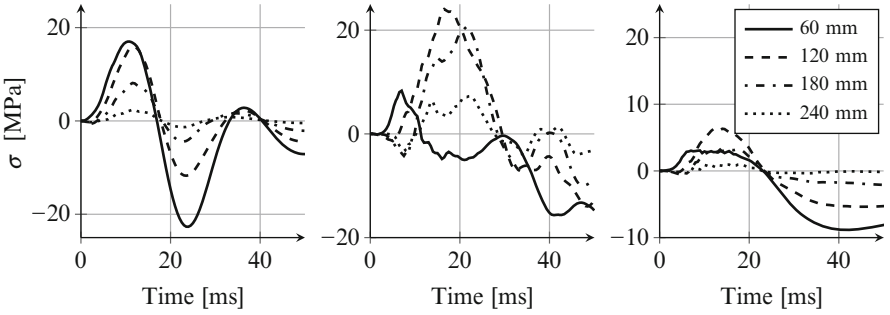

Fig. 39 Stresses at different distances from the wedge tip increasing the hydroelastic effect. A4-4 (*left*), A2-4 (*center*), V2-4 (*right*). $\beta = 30°$ ($V_0 = 4$ m/s)

Effects similar to the reduction of the deadrise angle are found by reducing the plate stiffness. Figure 39 shows a comparison of wedges with 30° deadrise angle and different stiffness entering the water at 4 m/s. Results show that moving from a stiffer plate (on the left, aluminum 4 mm thick plate) to a weaker plate (Fibreglass 2 mm thick, on the right), hydroelastic effects become more important and the deformations of the plate get more complicate since more vibrating modes superpose.

5.4 Influence of the Structural Deformation on the Impact Dynamics

As suggested in [16], the loading can be considered as quasi static if the loading period is significantly larger than the first natural period of the structure, otherwise

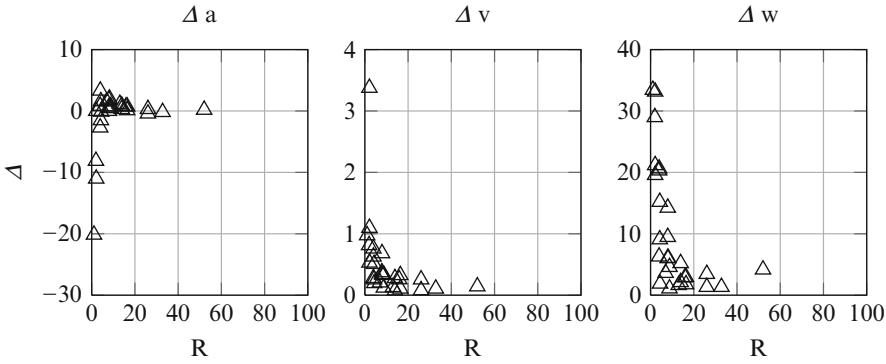

Fig. 40 Maximum impact dynamics variation between SPH results and Von Karman results. Acceleration a (m/s^2) (*left*), Velocity v (m/s) (*center*) and Displacement w (mm) (*right*)

hydroelastic effects might appear. Figure 40 shows the maximum variation with respect to Von Karman's results as function of the term R given by the ratio between the wetting time calculated as $\frac{tan(\beta)\cdot l}{v_0}$ and the first dry natural period of the structure calculated by the beam theory. β is the deadrise angle, v_0 is the impact velocity and l is the wedge side length. The numerical impact dynamics has been evaluated at the tip of the wedge. The calculation of the maximum variation between SPH and Von Karman results was calculated as:

$$\Delta a = max\left[a_{SPH}(t) - a_{th}(t)\right] \tag{17}$$

$$\Delta v = max\left[v_{SPH}(t) - v_{th}(t)\right] \tag{18}$$

$$\Delta w = max\left[w_{SPH}(t) - w_{th}(t)\right] \tag{19}$$

Results show that the impact dynamics differ from the Von Karman's analytical solution for values of R lower than 1, meaning that hydroelasticity needs to be taken into account when the wetting time is lower than the first structural dry natural period.

6 Comparison Between Experiments and Numerical Results

In the previous sections, experimental and numerical results were presented separately. In this section, the numerical results are compared with experiments.

Figures 41–43 show the comparison between experimental (blue lines) and numerical (red lines) results of the water-entry of elastic wedges. Figures 41 and 42 show the impact-induced stresses in an aluminum plate 2 mm thick with deadrise angle of 30° entering the water at 3 and 4 m/s. The numerical solutions compare well with the experimental results: stresses in time are well replicated both in terms of

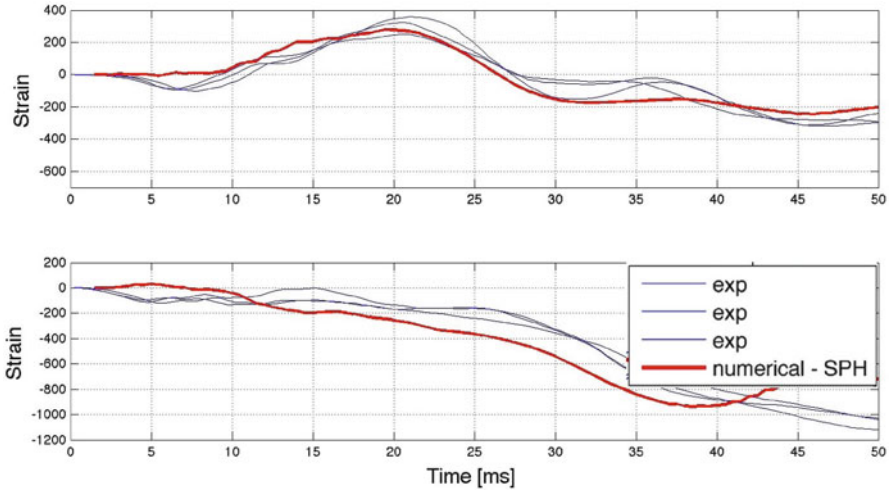

Fig. 41 Recorded strains and numerical solution of an aluminum wedge 2 mm thick, deadrise angle $\beta = 30°$. Initial velocity 3 m/s

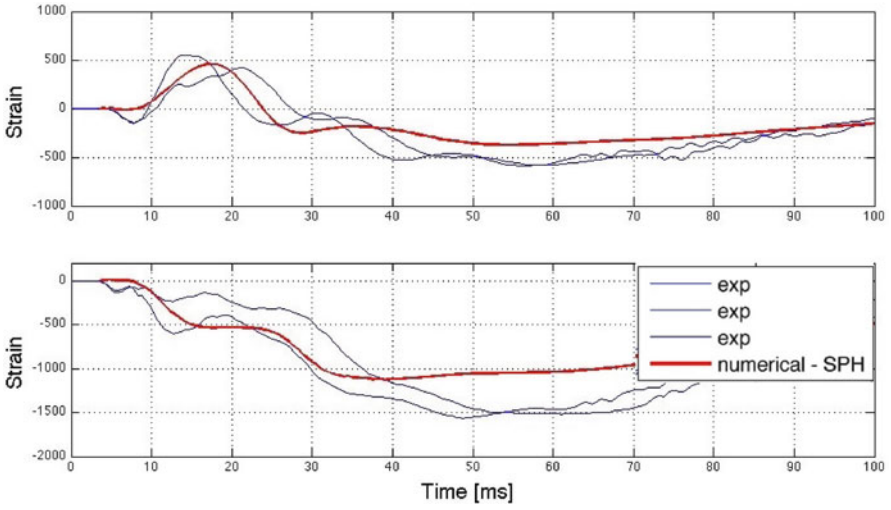

Fig. 42 Recorded strains and numerical solution of an aluminum wedge 2 mm thick, deadrise angle $\beta = 30°$. Initial velocity 4 m/s

maximum value and overall shape. This indicates that the simulations are correctly replicating the fluid/structure interaction in case of hydroelastic impacts. These results are particularly interesting considering that the panels are only 2 mm thick, deformations are consequently very high and the fluid motion is highly modified by the structure.

In Fig. 42 the numerical solution slightly differs from the experimentally recorded values after 40 ms of impact. This difference has to be attributed to

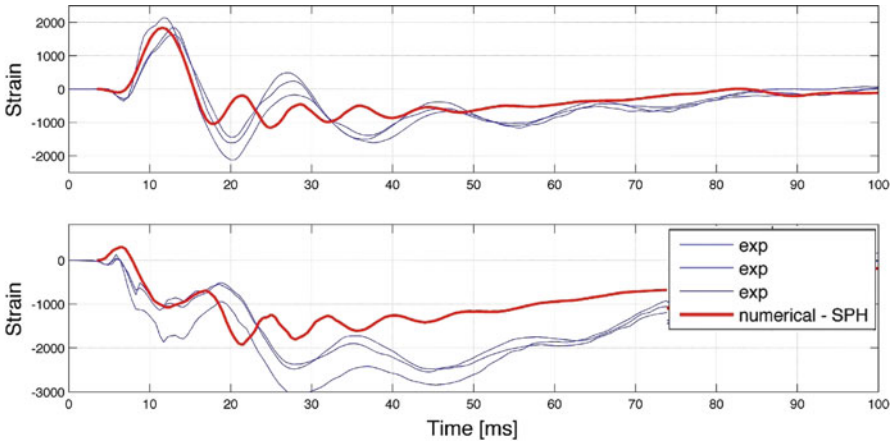

Fig. 43 Recorded strains and numerical solution of an aluminum wedge 2 mm thick, deadrise angle $\beta = 15°$. Initial velocity 5 m/s. Note that after 20 ms the experimental recorded strain show longer period of vibration compared to the numerical results

boundary effects: after 40 ms the entire wedge is wet and the water starts to overflow the panel from the side. To solve this problem the hydrodynamic loads acting on the free edge of the wedge have to be computed accurately. This can be done increasing the particle spatial resolution, with a consequent increase of the computational time. However, this problem is not on interest at this stage of the work.

Figure 43 shows the comparison between numerical and experimental results of an aluminum wedge 2 mm thick with deadrise angle of 15° entering the water at 5 m/s. In this case the numerical solution fits with the experiments only in the very first instants of the impact, approximately up to 20 ms. Later, the plates vibrates at higher frequencies in the numerical solution than in reality. In this simulation in fact the wedge detaches from the fluid and vibrates like in vacuum.

7 Conclusions

In this work, hydroelastic impacts of deformable wedges entering the water through free fall motion was studied numerically and experimentally. The water entry of rigid structures has been previously treated in the literature by other authors, however, on the contrary with their studies, this work investigates extremely flexible structures, introducing high hydroelastic effects. Furthermore, in opposition with what done in the literature, interest was pushed not only on the evaluation of the pressure at the fluid/structure interface but also on the overall structural deformation. Hydroelastic effects were studied as function of different parameters like: deadrise angle, impact velocity and plate stiffness to area mass ratio. In particular, it was found that hydroelastic effects lower increasing deadrise angle and plate stiffness,

while increase with the impact velocity. The relative importance of hydroelasticity was found to be governed by the ratio (R) between the wetting time and the natural period of the structure. For the particular geometry studied, hydroelasticity is important for values of R lower than 1.

The experiments were replicated by a numerical method. A coupled SPH/FEM model was used for the simulations and, validating the solutions with the experimental results, it was found that this model is actually capable of correctly modeling the fluid behavior and of predicting hydroelastic impacts, although a range of validity applies. For the cases studied, it was found that the structural deformation is not affecting the hydrodynamic pressure at the fluid/structure interface during the first instants of the impact: remarkable variations in the pressure at the fluid/structure interface appears only after the maximum impact force is reached. The presented SPH model was found to be able to simulate hydroelastic impacts if no air is trapped between the structure and the fluid. In fact, if (due to the structural deformation) air bubbles are trapped into the fluid during the impact, air cannot be neglected in the numerical model. By the numerical simulations it was also possible to better understand the mechanisms causing cavitation and air entrapment between the structure and the fluid due to hydroelastic effects.

Acknowledgements This research would not have been possible without the support and assistance of Prof. Serge Abrate, Prof. Giangiacomo Minak and Prof. Andrea Zucchelli, whose guidance and constant encouragement throughout the years will never be repaid enough.

Support from the Office of Naval Research (Grant n. N00014-12-1-0260) and the encouragement from the manager of the Solid Mechanics Program Dr. Yapa Rajapakse are gratefully acknowledged.

References

1. Von Karman TH (1929) The impact on seaplane floats, during landing. National Advisory Committee for Aeronautics, Washington, DC. NACA-TN-321
2. Mei X, Liu Y, Yue D (1999) On the water impact of general two-dimensional sections. Appl Ocean Res 21:1–15
3. Wagner H (1932) Uber Stoss-und Gleitvorgange an der Oberflache von Flussigkeiten. Z angew Math Mech 12(4):193–215
4. Daidola JC, Mishkevich V (1995) Hydrodynamic impact on displacement ship hulls: an assessment of the state of the art. Ship Structure Committee report SSC-385, NTIS PB96-129101
5. Korobkin A (2006) Second-order Wagner theory of wave impact. J Eng Math 58(1–4):121–139
6. Yettou E, Desrochers A, Champoux Y (2007) A new analytical model for pressure estimation of symmetrical water impact of a rigid wedge at variable velocities. J Fluids Struct 23(3):501–522
7. Judge C, Troesch A, Perlin M (2004) Initial water impact of a wedge at vertical and oblique angles. J Eng Math 48(3/4):279–303
8. Korobkin A (1988) Inclined entry of a blunt profile into an ideal fluid. Fluid Dyn 23(3):443–447
9. Riccardi G, Iafrati A (2004) Water impact of an asymmetric floating wedge. J Eng Math 49(1):19–39

10. Chekin B (1989) The entry of a wedge into an incompressible fluid. J Appl Math Mech 53(3):300–307
11. Qin Z, Batra R (2009) Local slamming impact of sandwich composite hulls. Int J Solids Struct 46(10):2011–2035
12. Korobkin A (2000) Unsteady hydroelasticity of floating plates. J Fluids Struct 14:971–991
13. Korobkin A, Khabakhpasheva T, Wu G (2008) Coupled hydrodynamic and structural analysis of compressible jet impact onto elastic panels. J Fluids Struct 24(7):1021–1041
14. Korobkin A, Guéret R, Malenica Š (2006) Hydroelastic coupling of beam finite element model with Wagner theory of water impact. J Fluids Struct 22(4):493–504
15. Iafrati A, Korobkin A (2008) Hydrodynamic loads during early stage of flat plate impact onto water surface. Phys Fluids 20(8):082104
16. Faltinsen O (2001) Hydroelastic slamming. J Mar Sci Technol 5(2):49–65
17. Korobkin A, Parau E, VandenBroeck J (2011) The mathematical challenges and modelling of hydroelasticity. Philos Trans Ser A Math Phys Eng Sci 369(1947):2803–2812
18. Chuang S (1970) Investigation of impact of rigid and elastic bodies with water. NSRDC report no. 3248
19. Carcaterra A, Ciappi E (2000) Prediction of the compressible stage slamming force on rigid and elastic systems impacting on the water surface. Nonlinear Dyn 21:193–220
20. Arai M, Miyanchi T (1998) Numerical study of the impact of water on cylindrical shells, considering fluid structure interactions. Dev Mar Technol 11:59–68
21. Kapsenberg G (2011) Slamming of ships: where are we now? Philos Trans Ser A Math Phys Eng Sci 369(1947):2892–2919
22. Faltinsen O (1997) The effect of hydroelasticity on ship slamming. Philos Trans R Soc A Math Phys Eng Sci 355(1724):575–591
23. Bereznitski A (2001) Slamming: the role of hydroelasticity. Int Shipbuild Prog 48(4):333–351
24. Carcaterra A (2004) Hydrodynamic shock of elastic structures impacting on the water: theory and experiments. J Sound Vib 271(1–2):411–439
25. Lu CH, HE YS, Wu GX (2000) Coupled analysis of nonlinear interaction between fluid and structure impact. J Fluids Struct 14:127–146
26. Peseux B, Gornet L, Donguy B (2005) Hydrodynamic impact: numerical and experimental investigations. J Fluids Struct 21(3):277–303
27. Scolan Y (2004) Hydroelastic behaviour of a conical shell impacting on a quiescent-free surface of an incompressible liquid. J Sound Vib 277(1–2):163–203
28. Charca S, Shafiq B, Just F (2009) Repeated slamming of sandwich composite panels on water. J Sandw Struct Mater 11(5):409–424
29. Charca S, Shafiq B (2009) Damage assessment due to single slamming of foam core sandwich composites. J Sandw Struct Mater 12(1):97–112
30. Hirdaris SE, Temarel P (2009) Hydroelasticity of ships: recent advances and future trends. Proc Inst Mech Eng Part M J Eng Marit Environ 223(3):305–330
31. Wu G (2004) Numerical simulation and experimental study of water entry of a wedge in free fall motion. J Fluids Struct 19(3):277–289
32. Seddon C, Moatamedi M (2006) Review of water entry with applications to aerospace structures. Int J Impact Eng 32(7):1045–1067
33. Stenius, I, Rosén A, Kuttenkeuler J (2011) Hydroelastic interaction in panel-water impacts of high-speed craft. Ocean Eng 38(2–3):371–381
34. Dalrymple RA, Rogers B (2006) Numerical modeling of water waves with the SPH method. Coast Eng 53(2–3):141–147
35. Oger G, Doring M, Alessandrini B, Ferrant P (2006) Two-dimensional SPH simulations of wedge water entries. J Comput Phys 213(2):803–822
36. Khayyer A, Gotoh H, Shao S (2008) Corrected Incompressible SPH method for accurate water-surface tracking in breaking waves. Coast Eng 55(3):236–250
37. Anghileri M, Castelletti L, Francesconi E, Milanese A, Pittofrati M (2011) Rigid body water impact: experimental tests and numerical simulations using the SPH method. Int J Impact Eng 38(4):141–151

38. Shao S (2009) Incompressible SPH simulation of water entry of a free-falling object. Int J Numer Methods Fluids 59:91–115
39. Battistin D, Iafrati A (2004) A numerical model for the jet flow generated by water impact. J Eng Math 48(3/4):353–374
40. Colagrossi A (2003) Numerical simulation of interfacial flows by smoothed particle hydrodynamics. J Comput Phys 191(2):448–475
41. Molteni D, Colagrossi A (2009) A simple procedure to improve the pressure evaluation in hydrodynamic context using the SPH. Comput Phys Commun 180(6):861–872
42. Geoffrey M, Smith PD (1995) Blast effects on buildings: design of buildings to optimize resistance to blast loading. T. Telford, London; American Society of Civil Engineers, New York
43. Korobkin A, Ellis AS, Smith FT (2008) Trapping of air in impact between a body and shallow water. J Fluid Mech 611:365–394
44. Chuang S, Milne D (1971) Drop tests of cone to investigate the three-dimensional effect of slamming. NRDC report no. 3543
45. Chuang S (1966) Slamming of rigid wedge-shaped bodies with various deadrise angles. NSRDC report 2268
46. Engle A (2003) A comparison of hydrodynamic impacts prediction methods with two dimensional drop test data. Mar Struct 16(2):175–182
47. Huera-Huarte FJ, Jeon D, Gharib M (2011) Experimental investigation of water slamming loads on panels. Ocean Eng 38(11–12):1347–1355
48. Lewis S, Hudson D, Turnock S, Taunton D (2010) Impact of a free-falling wedge with water: synchronized visualization, pressure and acceleration measurements. Fluid Dyn Res 42(3):035509
49. Inman D (1994) Engineering vibration. Vibration fundamentals and practice. Prentice Hall, Englewood Cliffs
50. Faltinsen O (1999) Water entry of a wedge by hydroelastic orthotropic plate theory. J Ship Res 43(3):180–193
51. Yupu G, Zhenhua Z, Wei C, Deping G (2008) Foreign object damage to fan rotor blades of aeroengine part II: numerical simulation of bird impact. Chin J Aeronaut 21(4):328–334
52. Brett J (1998) Numerical modeling of shock wave and pressure pulse generation by underwater explosion. Technical report, Department of Defence
53. Liu M, Liu G, Lam K (2002) Investigations into water mitigation using a meshless particle method. Shock Waves 12(3):181–195
54. Veen D, Gourlay T (2008) SPH study of high speed ship slamming. In: 3rd ERCOFTAC SPHERIC workshop on SPH applications, Lausanne
55. Khayyer A, Gotoh H, Shao S (2009) Enhanced predictions of wave impact pressure by improved incompressible SPH methods. Appl Ocean Res 31(2):111–131
56. Antoci C, Gallati M, Sibilla S (2007) Numerical simulation of fluid-structure interaction by SPH. Comput Struct 85(11–14):879–890
57. Marrone S, Antuono M, Colagrossi A, Colicchio G, Le Touzé D, Graziani G (2011) δ-SPH model for simulating violent impact flows. Comput Methods Appl Mech Eng 200(13–16):1526–1542
58. Johnson G (1996) Artificial viscosity effects for SPH impact computations. Int J Impact Eng 18(5):477–488
59. Nejad-Asghar M, Khesali AR, Soltani J (2007) Artificial viscosity in simulation of shock waves by smoothed particle hydrodynamics. Astrophys Space Sci 313(4):425–430
60. Mani A, Larsson J, Moin P (2009) Suitability of artificial bulk viscosity for large-eddy simulation of turbulent flows with shocks. J Comput Phys 228(19):7368–7374
61. Randles PW, Libersky LD (2000) Normalized SPH with stress points. Int J Numer Methods Eng 48(10):1445–1462
62. Selhammar M (1997) Modified artificial viscosity in smooth particle hydrodynamics. Astron Astrophys 325(2):857–865
63. Kai G, Hua L, Ben-long W (2009) Water entry of a wedge based on SPH model with an imporved boudary treatment. J Hydrodyn 21(6):750–757